AGU PUBLICATIONS

Tectonics

RESEARCH ARTICLE
10.1002/2015TC003855

Key Points:
- Tatry block was covered by up to 4 km of Paleogene sediments
- Tatry were exhumed mostly in the early and middle Miocene (~22 to 14 Ma)
- Exhumation of the Tatry records retrovergent thrusting within the overriding plate

Correspondence to:
M. Śmigielski,
m.j.smigielski@gmail.com

Citation:
Śmigielski, M., H. D. Sinclair, F. M. Stuart, C. Persano, and P. Krzywiec (2016), Exhumation history of the Tatry Mountains, Western Carpathians, constrained by low-temperature thermochronology, *Tectonics*, *35*, 187–207, doi:10.1002/2015TC003855.

Received 12 FEB 2015
Accepted 1 DEC 2015
Accepted article online 5 DEC 2015
Published online 23 JAN 2016

Exhumation history of the Tatry Mountains, Western Carpathians, constrained by low-temperature thermochronology

M. Śmigielski[1], H. D. Sinclair[2], F. M. Stuart[3], C. Persano[4], and P. Krzywiec[5]

[1]Piastów, Poland, [2]School of GeoSciences, University of Edinburgh, Edinburgh, UK, [3]Isotope Geosciences Unit, SUERC, East Kilbride, UK, [4]Department of Geographical and Earth Sciences, University of Glasgow, Glasgow, UK, [5]Institute of Geological Sciences, Polish Academy of Sciences, Warszawa, Poland

Abstract This study tests alternative models for the growth of the Tatry Mountains (Central Western Carpathians) by the application of low-temperature thermochronology. Zircon (U + Th)/He ages from the north of the range are mostly between 48 and 37 Ma and indicate cooling prior to the onset of fore-arc sedimentation in the region (42–39 Ma). In contrast, zircon (U + Th)/He ages in the south of the range are around 22 Ma. Apatite fission track ages across the sampled sites range from 20 to 15 Ma. Apatite (U + Th)/He ages range from 18 to 14 Ma with little variation with elevation or horizontal location. Based on thermal modeling and tectonic reconstructions, these Miocene ages are interpreted as cooling in the hanging wall of a northward dipping thrust ramp in the current location of the sub-Tatric fault with cooling rates of ~20°C/Myr at ~22–14 Ma. Modeled cooling histories require an abrupt deceleration in cooling after ~14 Ma to <5°C/Myr. This is associated with termination of deformation in the Outer Carpathians and is synchronous with the transition of the Pannonian Basin from a syn-rift to a postrift stage and with termination of N-S compression in the northern part of the Central Western Carpathians. Overall, the timing of shortening and exhumation is synchronous with the formation of the Outer Carpathian orogen and so the Miocene exhumation of the Tatry records retrovergent thrusting at the northern margin of the Alcapa microplate.

1. Introduction

Alpine orogenesis across Europe has resulted in a wide range of tectonic interactions between regions of crustal thickening at convergent boundaries and thinning associated with slab retreat and mantle instability. Mountain ranges such as the Betic-Rif system and its association with extension in the Alboran Sea in western Europe have generated much debate concerning their geodynamic origins [*Platt and England*, 1994; *Lonergan and White*, 1997]. A similarly spectacular example of the proximal synchroneity of lithospheric thickening and extension comes from the formation of the Carpathian arc and the Pannonian Basin of eastern Europe in Miocene times [*Ślączka et al.*, 2005; *Tari and Horváth*, 2005]. The formation of the Outer Carpathian thrust wedge at the same time as extension in the Pannonian Basin has been interpreted to have resulted from the northward rollback of the subducting European lithosphere starting at ~20 Ma [*Royden et al.*, 1983; *Horváth*, 1993] with arc volcanism and back-arc rifting in the Pannonian Basin lasting until around 11 Ma. An alternative tectonic model for the Carpathian thrust wedge/Pannonian Basin system is that it results from gravitational instability of the mantle lithosphere following thickening [*Houseman and Gemmer*, 2007].

The pre-Miocene evolution of the Carpathians is dominated by Cretaceous orogenesis involving Variscan basement massifs and the development of complex fold nappes of Mesozoic sediments of the Central Western Carpathians (CWC) [*Plašienka et al.*, 1997]. The Tatry Mountains of southern Poland and northern Slovakia contain the highest peaks of the Carpathian mountain chain, and they are an important component of this larger system (Figure 1). The CWC forms the boundary between the Miocene extensional regime of the Pannonian Basin and the Outer Carpathian thrust wedge, so understanding the evolution of the Tatry is critical to understanding the relationship between contraction and extension at this time (Figure 1).

The Tatry massif is surrounded by a deformed sedimentary succession of the Central Carpathian Paleogene Basin (CCPB) that is thought to represent the former fore-arc basin of the Carpathian orogenic belt [*Kázmér et al.*, 2003] (Figure 1). The massif belongs to the overriding southern plate and is located close to its northern edge, ~20 km south from the Pieniny Klippen Belt; a suture belt that probably represents a remnant of a collision zone of the European plate and Alcapa terranes [*Oszczypko et al.*, 2010]. The

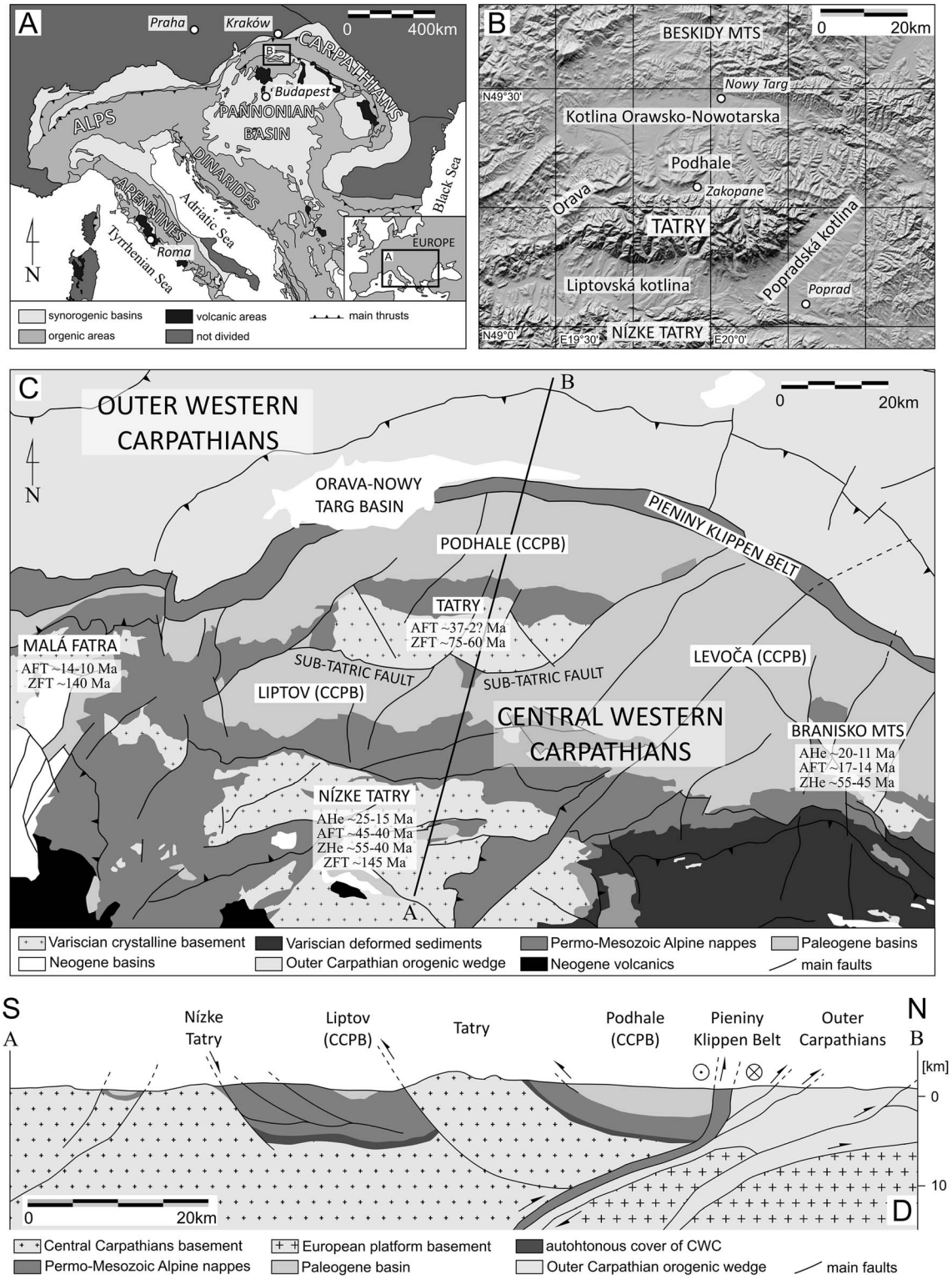

Figure 1. Geology of the Tatry area. (a) Map of the main geological structures of the central and southern Europe [after *Oszczypko et al*., 2006]. (b) Shaded relief image of the Digital Elevation Model (3″ × 3″) of the Tatry mountains and surrounding areas. (c) Geological map of the Central Western Carpathians in the Tatry region (after *Lexa et al*. [2000], simplified). The thermochronologic ages are after: Malá Fatra - *Danišík et al*. [2010] and *Králiková et al*. [2014b]; Nízke Tatry - *Danišík et al*. [2011]; Branisko Mountains - *Danišík et al*. [2012]; Tatry - *Burchart* [1972], *Král'* [1977], *Baumgart-Kotarba and Král* [2002], *Anczkiewicz et al*. [2005], and *Králiková et al*. [2014a]. (d) Schematic cross section through the Tatry and surrounding areas (after *Schmid et al*. [2008], modified).

Pieniny Klippen Belt forms the boundary between the Central Western Carpathians and the Outer Carpathians orogenic wedge (Figure 1).

In this paper we present a low-temperature thermochronology study of the high-elevation region of the Tatry massif using all established techniques. Apatite fission track (AFT) and (U + Th)/He analysis in apatites and zircons (AHe and ZHe) are now routinely used to identify periods of rapid cooling and relative displacements across major structures in mountain ranges [e.g., *Reiners and Brandon*, 2006; *Kirstein et al*., 2006; *Foeken et al*., 2007]. Here we use cooling histories determined from the three thermochronometers to test contrasting tectonic models for the formation of the Tatry mountains, in particular, to address whether they are formed by footwall uplift linked to normal faulting or thrusting due to Palaeogene or Neogene crustal thickening [*Sperner et al*., 2002; *Jurewicz*, 2005]. The new thermal history for the region is discussed in the context of the development of the Outer Carpathians and the Pannonian Basin and yields insight into the geodynamic linkage between these two systems [*Ratschbacher et al*., 1991].

2. Geological Background

The Tatry massif forms an east-west trending range approximately 60 km long and 15 km wide, comprising a "core and cover" structure similar to other Variscan massifs of the Central Western Carpathians [*Plašienka et al*., 1997]. Carboniferous granites that intrude lower Paleozoic metasedimentary rocks dominate the southern part of the range, forming the highest peaks [*Jurewicz*, 2005; *Burda et al*., 2013] (Figure 1). The Paleozoic basement is overlain by autochthonous Permo-Triassic conglomerates and sandstones that form the base of a stack of nappes of Triassic to Cretaceous sedimentary rocks [*Plašienka et al*., 1997; *Rubinkiewicz and Ludwiniak*, 2005]. These nappes are best exposed on the northern slopes of the range. The nappes were formed and thrust northward during the Alpine orogeny (late Cretaceous) when several terranes (the Alcapa microplate) collided with the European plate [*Csontos and Vörös*, 2004]. At that time, the CWC range was located in the eastern part of the Alpine collision zone and was later extruded toward the northeast [*Ratschbacher et al*., 1991]. Between 1 and 3 km of sediments of the original Mesozoic nappe stack are preserved on the northern slope of the mountains (Figure 1). K-Ar dating suggests that the Tatry granite has not exceeded ~250°C (~10 km burial) since Permian times [*Kováč et al*., 1994, and references therein]. This is consistent with petrologic data that indicate that the pressure might have been close to 250 MPa (~10 km burial) [*Petrík et al*., 2003] and concurs with recent zircon fission track data [*Králiková et al*., 2014a].

North of the Tatry, the Alpine basement is unconformably overlain by Eocene to early Miocene Central Carpathian Paleogene Basin sediments [e.g., *Roniewicz*, 1969]. The Tatry massif is separated from the CCPB sediments to the south, west, and east by faults (Figure 1c). The CCPB was a fore-arc basin that developed on the overriding plate close to the subduction zone responsible for forming the Outer Carpathian orogenic wedge [e.g., *Kázmér et al*., 2003]. Marine transgression in the Tatry area occurred at 42–39 Ma, and deep marine sedimentation was established at ~35 Ma [*Bartholdy et al*., 1999; *Soták*, 2010; *Starek et al*., 2012]. The absence of pebbles of basement granites in the conglomerates of the CCPB, and paleocurrent reconstructions, suggest that the Tatry was not an important source of sediments during Eocene-Oligocene or that only the Mesozoic nappes were exposed at this time [e.g., *Soták et al*., 2001]. Approximately 3.5 km of CCPB sediments are preserved in the Podhale syncline north of the Tatry [*Ludwiniak*, 2010]. Sedimentation in the CCPB (Figure 1d) lasted until at least ~23 Ma [*Gedl*, 2000; *Soták et al*., 2001; *Garecka*, 2005]. It is likely that the youngest part of the CCPB succession was eroded in Neogene times [*Środoń et al*., 2006]; thus, the complete sedimentation history of the CCPB is unclear.

Shortening of the western segment of the Outer Carpathians started in Eocene/Oligocene times, but the peak of thrusting was at ~25–15 Ma [*Gągała et al*., 2012; *Andreucci et al*., 2013]. Thrusting was accompanied by the formation of the Carpathian foredeep basin [*Oszczypko*, 2006]. In the sector of the Outer Carpathian belt located to the north of the Tatry, the main thrusting phase ceased after ~13.6 Ma [*Nemčok et al*., 2006a, 2006b] and the final stages of tectonic activity within the frontal orogenic wedge took place after ~12 Ma [*Krzywiec et al*., 2014].

The shortening in the Outer Carpathians was accompanied by extension in the Pannonian region (~100 km south of the Tatry) where a back-arc basin formed at ~20–17.5 Ma due to slab rollback and asthenospheric upwelling [*Royden et al*., 1983; *Horváth*, 1993] (Figure 1a). The syn-rift stage of the basin development

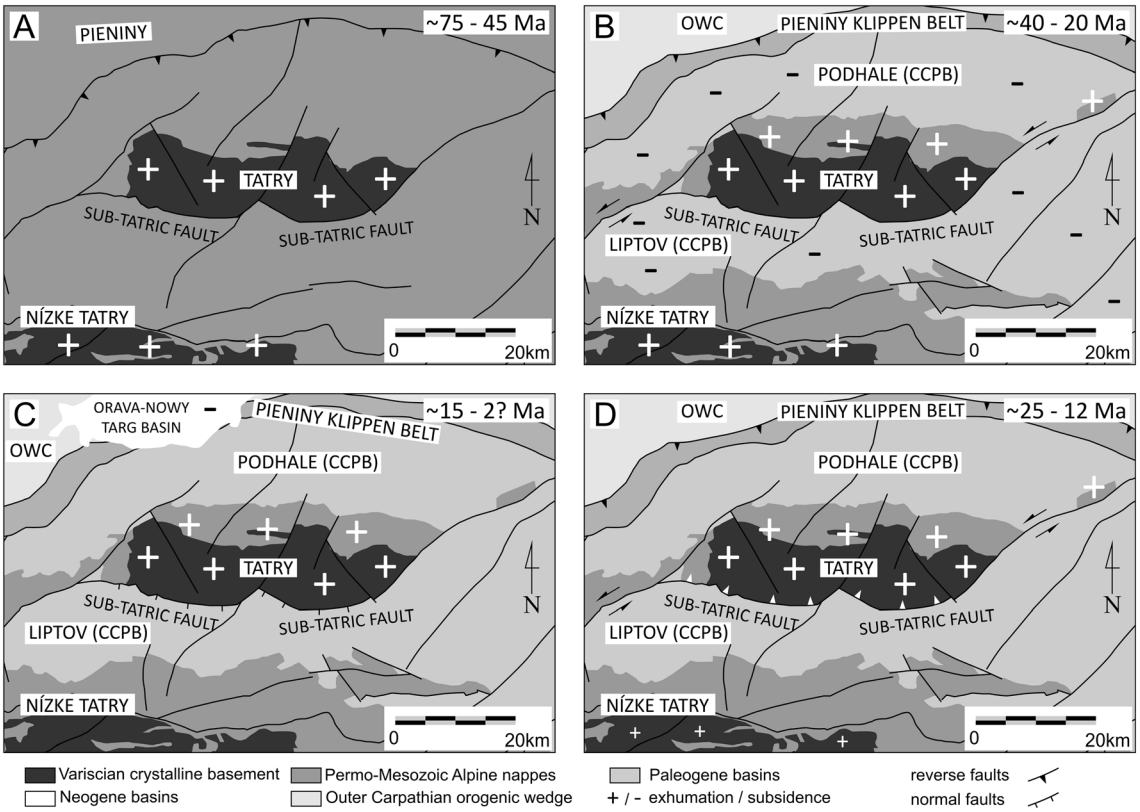

Figure 2. Four hypothetical end-member models of the exhumation history of the Tatry. (a) Model 1. Inherited Cretaceous-Palaeogene Alpine deformation with minor Neogene rejuvenation, similarly to the exhumation history of the Nízke Tatry massif to the south of the Tatry. (b) Model 2. Late Eocene-early Oligocene faulting synchronous with the sedimentation in the CCPB that continued into the Miocene. (c) Model 3. Extensional footwall uplift during Miocene/Pliocene. For the cross-section view see Figure 6a. (d) Model 4. Backthrusting during Carpathian orogenesis in early-middle Miocene. For the cross-section view see Figures 6b and 7. Please note that simplified geological maps presented on this figure do not show paleoreconstructions. For more explanations and references, see text.

lasted until 11.5–10.5 Ma [*Houseman and Gemmer*, 2007]. Subduction of the European plate margin along with lateral extrusion of the Alcapa block and mantle diapiric upwelling produced calc-alkaline volcanism from 20 Ma to 11 Ma. This was followed by intermittent alkalic basaltic volcanism until 0.5 Ma [*Seghedi et al.*, 2005].

The tectonic evolution of the Tatry is critical to understanding the Cenozoic development of the CWC. However, there is little consensus on the underlying controls. The last large-scale tectonic modification of the Tatry is recorded by the northward tilting (~40°) of the transgressive Eocene sediments that overlie the northern margin of the Tatry [*Mastella*, 1975] (Figure 1d). The basal Triassic conglomerates that sit on the granites also dip 40° to the north [*Rubinkiewicz and Ludwiniak*, 2005]. As the Mesozoic nappes form the basement of the CCPB the tilt might be related to the formation of the Podhale syncline in Neogene times [*Plašienka et al.*, 2001; *Szaniawski et al.*, 2012] (Figure 1d). The structure of the core of the Tatry is not clear. The biggest unknown is the geometry and kinematics of the W-E trending sub-Tatric fault. The fault forms the southern boundary of the massif and is likely to has been a key control on the exhumation of the Tatry massif (Figure 1c). The fault is poorly exposed because of the cover of Quaternary glaciogenic sediments. Of the many hypotheses that have been put forward regarding the fault geometry, two are the most established. The sub-Tatric fault could be either a steep north dipping reverse fault [e.g., *Sperner*, 1996; *Plašienka et al.*, 2001] or a south dipping normal fault [e.g., *Hrušecký et al.*, 2002; *Jurewicz*, 2005]. A hypothesis that fault kinematics changed substantially over time has also been proposed [*Králiková et al.*, 2014a].

Previous thermochronology studies have not produced a consistent cooling history (Figure 1). These studies are largely restricted to apatite fission track determinations and imply that major cooling and denudation of

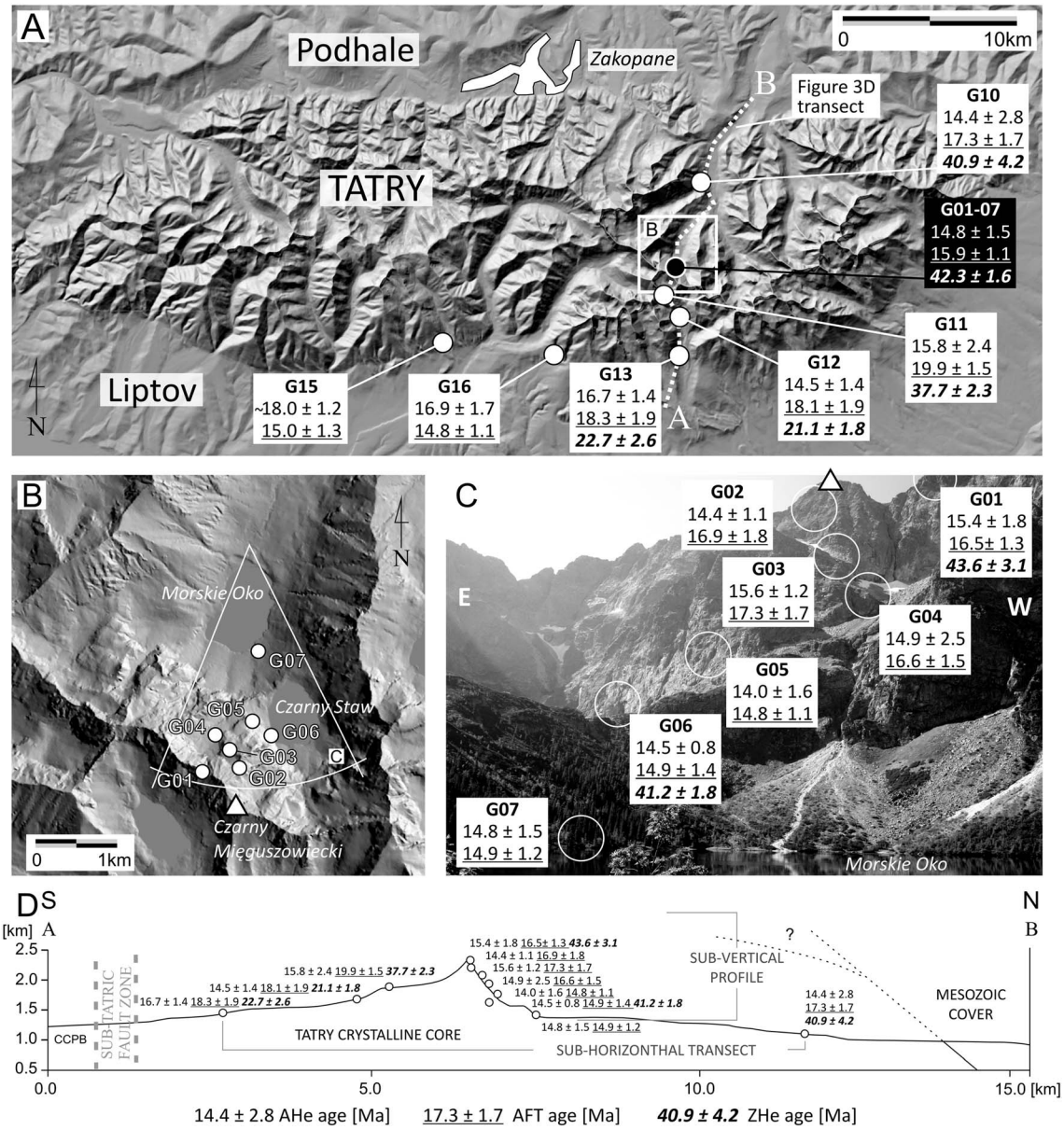

Figure 3. Spatial distribution of the thermochronological data. (a) Shaded relief image of the Digital Elevation Model (1″ × 1″) from the Tatry area. White circles: location of sampling sites, black circle: location of subvertical sampling profile. Sample name and average thermochronological ages are given in rectangles: normal font, AHe; underlined font, AFT; italics, ZHe. For the subvertical profile presented ages are averaged for the whole profile. White dashed line shows the line of the topographic cross section (D). (b) Shaded relief image of the Digital Elevation Model (10 m × 10 m) from the Czarny Staw area. White circles - location of sampling sites. White angle shows the view area of the picture presented in the part C. (c) Photograph of the Morskie Oko valley and lake. White circles - location of sampling sites. Sample name and average thermochronological ages are given in rectangles: normal font, AHe; underlined font, AFT; italics, ZHe. (d) Topographic profile with localization of sampling sites in the subvertical and subhorizontal sampling profiles through the Tatry (for location see A). Average thermochronological ages are given: normal font, AHe; underlined font, AFT; italics, ZHe. CCPB - Central Carpathian Paleogene Basin. Dashed line shows unknown, possible position of the Mesozoic cover of the Tatry crystalline core.

the Tatry appears to have occurred between ~37 and ~2 Ma. The earliest AFT analysis by *Burchart* [1972] and by *Král'* [1977] yielded cooling ages of between ~20 and ~10 Ma although 30 to 37 Ma cooling ages were measured in the northern part of the massif. The uncertainties on the age estimations are 15% to 40% [*Burchart*, 1972]. More recent AFT analyses were performed by *Baumgart-Kotarba and Král* [2002] and *Anczkiewicz et al*. [2005]. The first survey was based on four samples collected along the sub-Tatric fault that recorded AFT ages from ~7 Ma to ~2 Ma [*Baumgart-Kotarba and Král*, 2002]. The second was based on 37

Table 1. Apatite (U + Th)/He Results From Samples From Tatry Mountains[a]

sample name	replicate	238U (ng)	±1σ error (%)	232Th (ng)	±1σ error (%)	4He (ncc/mg)	±1σ error (%)	Th/U	Raw Age (Ma)	F_T	Corrected age (Ma)	±1σ (Ma)
G_01	1	0.019	15.7%	0,068	9,7%	10.2	2.0%	3.61	9.5	0.75	12.7	1.2
	2	0.097	3.5%	-	-	63.1	1.0%	-	11.4	0.72	15.8	0.6
	4	0.223	2.3%	0,057	11,5%	108.9	0.6%	0.25	11.2	0.74	15.2	0.4
	5	0.140	2.8%	0,035	18,4%	66.6	0.7%	0.25	13.7	0.77	17.8	0.5
	6	0.060	5.2%	0,040	16,1%	35.2	1.2%	0.68	11.8	0.74	15.9	0.8
											15.4 ± 1.8 Ma	
G_02	2	0.381	3.2%	0,104	6,4%	49.5	0.5%	0.27	11.9	0.83	14.3	0.5
	4	0.313	2.8%	0,044	14,7%	101.2	0.5%	0.14	11.9	0.76	15.6	0.4
	5	0.256	2.4%	0,089	7,5%	86.5	0.6%	0.35	10.2	0.76	13.4	0.3
											14.4 ± 1.1 Ma	
G_03	2	0.025	11.6%	0,118	5,7%	11.7	1.2%	4.64	11.1	0.80	13.9	0.9
	4	0.174	2.5%	0,030	21,4%	85.4	0.6%	0.17	11.4	0.75	15.2	0.4
	6	0.249	2.2%	0,085	7,8%	88.8	0.5%	0.34	12.5	0.76	16.4	0.4
	7	0.043	7.0%	-	-	20.2	1.3%	-	13.1	0.76	17.2	1.2
	8	0.074	4.3%	-	-	34.0	0.9%	-	11.5	0.74	15.6	0.8
											15.6 ± 1.2 Ma	
G_04	3	0.028	10.5%	0,044	14,9%	28.2	1.5%	1.55	12.4	0.71	17.4	1.5
	4	0.090	3.7%	0,010	61,8%	24.1	0.9%	0.12	9.7	0.78	12.4	0.5
	6	0.034	8.7%	0,018	35,0%	15.5	1.5%	0.54	11.7	0.77	15.2	1.4
											14.9 ± 2.5 Ma	
G_05	1	0.128	2.9%	0,113	6,0%	42.7	0.7%	0.88	9.2	0.77	12.0	0.3
	2	0.354	2.3%	0,042	15,4%	161.4	0.5%	0.12	11.0	0.74	14.9	0.4
	3	0.069	4.6%	0,142	4,8%	26.5	0.8%	2.07	10.0	0.77	13.0	0.5
	4	0.281	2.2%	0,028	23,0%	144.0	0.6%	0.10	12.2	0.75	16.2	0.4
	9	0.634	3.1%	0,170	4,1%	98.4	0.5%	0.27	11.9	0.83	14.3	0.4
											14.0 ± 1.6 Ma	
G_06	1	0.444	2.8%	0,025	25,7%	73.5	0.5%	0.06	12.5	0.83	15.1	0.4
	3	1.214	4.9%	0,231	3,1%	175.5	0.5%	0.19	11.4	0.82	13.9	0.7
	~~5~~	~~0.171~~	~~2.7%~~	~~0,250~~	~~3,0%~~	~~46.4~~	~~0.8%~~	~~1.46~~	~~4.9~~	~~0.74~~	~~6.6~~	~~0.2~~
											14.5 ± 0.8 Ma	
G_07	1	0.164	2.8%	0,022	30,1%	68.5	0.6%	0.13	10.5	0.76	13.8	0.4
	7	0.077	4.2%	-	-	21.4	0.8%	-	13.2	0.80	16.5	0.8
	9	0.300	2.3%	0,045	14,5%	88.7	0.5%	0.15	11.0	0.77	14.3	0.3
											14.8 ± 1.5 Ma	
G_10	1	0.129	2.9%	0,036	18,2%	41.7	0.6%	0.27	13.5	0.79	17.1	0.5
	7	0.391	2.9%	0,071	9,2%	134.3	0.5%	0.18	11.6	0.77	15.0	0.4
	9	0.075	4.3%	0,199	3,6%	31.1	0.8%	2.66	9.0	0.78	11.5	0.4
											14.4 ± 2.8 Ma	
G_11	1	0.009	23.5%	0,020	25,2%	32.6	1.5%	2.12	9.1	0.55	16.5	2.9
	~~2~~	~~0.043~~	~~5.2%~~	~~0,017~~	~~30,4%~~	~~105.9~~	~~0.6%~~	~~0.38~~	~~15.6~~	~~0.61~~	~~25.5~~	~~1.4~~
	3	0.019	11.4%	-	-	34.6	1.0%	-	11.6	0.62	18.7	2.1
	4	0.050	2.3%	0,042	9,2%	74.9	0.6%	0.84	7.5	0.57	13.1	0.3
	5	0.072	1.8%	0,044	8,7%	81.5	0.6%	0.62	9.7	0.64	15.2	0.3
											15.8 ± 2.4 Ma	
G_12	1	0.069	3.4%	-	-	94.8	0.6%	-	10.5	0.63	16.7	0.6
	2	0.420	1.3%	0,047	10,8%	256.9	0.5%	0.11	9.7	0.68	14.2	0.2
	3	0.288	1.4%	0,019	26,9%	226.5	0.5%	0.06	10.4	0.69	15.0	0.2
	4	0.365	2.0%	0,076	5,2%	208.5	0.5%	0.21	10.2	0.72	14.2	0.3
	5	0.121	1.5%	0,050	7,8%	86.8	0.5%	0.41	8.7	0.68	12.8	0.2
											14.5 ± 1.4 Ma	
G_13	1	0.018	12.1%	-	-	15.8	2.1%	-	12.0	0.70	17.1	2.1
	2	0.017	12.9%	-	-	11.9	2.5%	-	10.8	0.71	15.2	2.2
	3	0.013	16.6%	-	-	24.8	3.2%	-	10.7	0.60	17.9	3.0
	~~4~~	~~0.004~~	~~51.5%~~	-	-	~~19.1~~	~~3.8%~~	-	~~28.5~~	~~0.62~~	~~45.9~~	~~23.8~~
	~~5~~	~~0.007~~	~~31.4%~~	-	-	~~22.3~~	~~5.4%~~	-	~~11.9~~	~~0.52~~	~~22.9~~	~~7.3~~
											16.7 ± 1.4 Ma	
G_15	1	0.017	6,0%	0,020	18,9%	22.3	2.6%	1.21	11.8	0.66	17.9	1.2
	~~3~~	~~0.021~~	~~10,8%~~	-	-	~~42.0~~	~~1.4%~~	-	~~22.0~~	~~0.68~~	~~32.3~~	~~3.7~~
	4	0.093	2,7%	-	-	91.5	0.7%	-	12.3	0.68	18.1	0.5
	~~5~~	~~0.013~~	~~17,4%~~	-	-	~~50.3~~	~~2.7%~~	-	~~19.1~~	~~0.56~~	~~34.1~~	~~6.0~~
											18.0 ± 1.2 Ma	
G_16	1	0.046	2,4%	0,012	32,1%	40.8	1.0%	0.26	10.5	0.67	15.6	0.5
	2	0.042	2,6%	-	-	51.8	0.9%	-	12.7	0.67	18.9	0.7
	~~3~~	~~0.078~~	~~1,7%~~	~~0,006~~	~~59,3%~~	~~129.4~~	~~0.5%~~	~~0.08~~	~~21.6~~	~~0.69~~	~~31.3~~	~~0.7~~
	4	0.040	2,7%	0,005	79,7%	63.9	1.1%	0.12	9.9	0.60	16.5	0.6
											16.9 ± 1.7 Ma	

[a] ^{238}U: mass of ^{238}U; ^{232}Th: mass of ^{232}Th; ^{4}He: ^{4}He volume per nano cm^3 STP; Th/U: ^{232}Th to ^{238}U factor; F_T: alpha recoil correction factor after *Farley et al.* [1996]; corrected age (Ma): corrected He age; ±1σ: sigma standard deviation of corrected age. Bold, average age of sample and ±1σ standard deviation based on geometric average. Strikethrough, values removed from the dataset. For more explanations see text.

Table 2. Apatite Fission Track Results From Samples From Tatry Mountains[a]

Sample	N	ρ_s (10^5/cm^2)	N_s	ρ_i (10^5/cm^2)	N_i	ρ_d (10^5/cm^2)	N_d	P (χ^2) (%)	Dpar (μm)	±1σ (μm)	Age (Ma)	±1σ (Ma)
G_01	20	1.58	175	27.83	3080	15.18	14313	99.9	1.82	0.21	16.5	1.3
G_02	21	1.34	1665	23.44	1665	16.13	14313	25.7	1.55	0.12	16.9	1.8
G_03	11	2.88	111	49.16	1898	16.14	14313	1.9	1.9	0.10	17.3	1.7
G_04	20	1.16	136	20.62	2420	20.62	14313	99.9	1.89	0.17	16.6	1.5
G_05	20	2.21	225	43.92	4467	16.10	14313	38.9	1.78	0.19	14.8	1.1
G_06	19	2.52	131	50.00	2601	16.10	14313	99.9	1.95	0.24	14.9	1.4
G_07	20	1.43	184	28.64	3675	16.10	14313	5.8	1.69	0.27	14.9	1.2
G_10	19	1.82	111	31.16	1897	16.11	14313	99.1	1.63	0.22	17.3	1.7
G_11	20	2.02	219	28.85	3131	15.50	10014	99.9	1.96	0.11	19.9	1.5
G_12	20	1.15	103	17.82	1596	15.30	10014	99.9	1.81	0.10	18.1	1.9
G_13	20	1.02	99	15.69	1520	15.30	10014	99.9	1.84	0.05	18.3	1.9
G_15	20	0.93	141	17.54	1662	15.40	10014	99.5	1.91	0.10	15.0	1.3
G_16	20	1.43	209	26.81	3919	15.10	10014	99.9	1.86	0.20	14.8	1.1

[a]N: number of crystals; ρ_s: spontaneous track density (per cm^2); N_s: number of counted spontaneous tracks; ρ_i: inducted track density (per cm^2); N_i: number of counted inducted tracks; ρ_d: dosimeter track density (per cm^2); N_d: number of tracks counted on dosimeter; P (χ^2): probability for obtaining chi-square value for single population test; Dpar: value of average etch pit diameter of fission tracks, Durango apatite standard Dpar: 1.81 ± 0.1 [*Carlson et al.*, 1999]; ±1σ (μm): standard deviation for Dpar. Age: central age; ±1σ (Ma): sigma error for age.

samples collected through the Tatry. In the eastern part of the massif the AFT ages are from 9 Ma to 21 Ma with the peak between ~15 Ma and ~10 Ma. In the western part of the massif the ages are from 12 Ma to 31 Ma with a peak between ~18 and ~31 Ma [*Anczkiewicz et al.*, 2005]. The most recently published study covers the southeastern part of the Tatry where four samples yield AFT ages from 12 Ma to 9 Ma and was supported by the Zircon Fission Track (ZFT) analysis that record ages of ~75–60 Ma [*Králiková et al.*, 2014a].

The Tatry is the highest of several granitic massifs of the CWC (Figure 1c). The Malá Fatra massif to the west of the Tatry experienced major cooling in mid-Miocene times [*Danišík et al.*, 2010; *Králiková et al.*, 2014b] (Figure 1c). The Nízke Tatry Mountains to the south are characterized by a rapid Paleogene cooling from 55–40 Ma with Miocene AHe ages between 20 and 15 Ma and a reduction in cooling rates since then [*Danišík et al.*, 2011]. The Branisko Mountains to the east record a mid-Miocene thermal event but also contain late Cretaceous-Eocene ZHe ages, which have been interpreted as cooling ages related to postorogenic exhumation after the mid-Cretaceous Alpine collision [*Danišík et al.*, 2012]. These data imply that the Central Western Carpathian massifs have experienced a rather complicated thermal history comprising Mesozoic tectonosedimentary burial [*Kováč et al.*, 1994; *Plašienka et al.*, 1997], possible postorogenic exhumation in late Mesozoic to early Paleogene times, followed by another burial/exhumation event in Paleogene to early-middle Neogene times [*Danišík et al.*, 2004]. The thermal history of the region has also been influenced by an elevated geothermal gradient related to the Miocene volcanism, referred to as the "mid-Miocene thermal event" [*Danišík et al.*, 2012; *Anczkiewicz et al.*, 2013].

Based on the proposed tectonic models for the evolution of the Tatry, in addition to the published thermochronometric data from the Tatry and surrounding massifs, we have derived four different end-member solutions for the Tatry exhumation (Figure 2). These preliminary models will be tested and discussed later in the paper.

3. Samples and Methodology

Thirteen samples of granite-granodiorite from the pre-Alpine basement of the Tatry were collected along three transects: (1) N-S transect ~10 km long through the massif from Wodogrzmoty Mickiewicza falls to Štrbské Pleso lake (eleven samples), (2) subvertical transect ~1 km high from Morskie Oko lake to the peak of Mięguszowiecki (seven samples), (3) E-W transect ~14 km along the sub-Tatric fault at the southern margin of the mountains (three samples). Sample locations are shown in Figure 3.

Here we present AFT and AHe data from all the 13 samples and ZHe ages from six strategically selected samples. For the AHe and ZHe methods, single, euhedral, inclusion-free crystals were handpicked, measured, and packed in Pt foil tubes. Helium was extracted by heating the Pt foils with a 808 nm diode laser at 600–700°C for 60 s

Table 3. Zircon (U + Th)/He Results From Samples From Tatry Mountains[a]

Sample Name	Replicate	^{238}U (ng)	±1σ Error (%)	^{232}Th (ng)	±1σ Error (%)	^{4}He (ncc/mg)	±1σ Error (%)	Th/U	Raw Age (Ma)	F_T	Corrected Age (Ma)	±1σ (Ma)
G_01	1	0.521	1.2%	0.126	8.3%	746.7	0.5%	0.24	24.8	0.61	40.7	0.6
	2	20.695	1.1%	0.395	2.8%	1929.0	0.5%	0.15	33.8	0.72	46.9	0.6
									43.6 ± 3.1 Ma		**43.7 ± 4.4 Ma**	
G_06	1	1.532	1.6%	0.394	1.6%	891.4	0.5%	0.26	24.3	0.64	37.9	0.6
	4	0.620	1.3%	0.235	2.3%	755.8	0.5%	0.38	22.9	0.52	44.0	0.6
	2	0.778	1.3%	0.284	2.0%	662.1	0.5%	0.37	24.2	0.58	41.7	0.6
									41.2 ± 1.8 Ma		**41.1 ± 3.1 Ma**	
G_10	1	0.331	1.4%	0.062	16.5%	345.5	0.5%	0.19	13.3	0.57	23.4	0.4
	2	0.919	1.2%	0.102	10.0%	1275.8	0.5%	0.11	23.3	0.61	38.2	0.5
	3	0.480	1.2%	0.044	23.2%	1095.2	0.5%	0.09	29.5	0.55	53.7	0.8
	4	2.823	1.2%	0.668	2.5%	656.4	0.5%	0.24	29.8	0.80	37.3	0.5
	5	1.634	1.2%	0.496	2.6%	904.7	0.5%	0.30	30.9	0.74	41.8	0.5
	6	3.628	1.1%	0.314	3.4%	1295.6	0.4%	0.09	25.1	0.75	33.5	0.4
	7	0.921	1.1%	0.293	3.5%	965.4	0.5%	0.32	51.1	0.74	69.0	0.8
	8	2.798	1.2%	0.734	2.4%	2020.4	0.5%	0.26	24.9	0.67	37.1	0.4
	9	1.865	1.2%	0.326	3.3%	1370.3	0.5%	0.17	34.4	0.72	47.8	0.6
									40.9 ± 4.2 Ma		**40.7 ± 13.1 Ma**	
G_11	4	3.300	1.2%	1.115	2.2%	1386.1	0.5%	0.34	34.0	0.76	44.7	0.6
	5	2.400	1.2%	0.528	2.6%	1134.3	0.5%	0.22	23.2	0.73	31.8	0.4
	6	2.173	1.1%	0.386	2.9%	923.0	0.5%	0.18	24.6	0.74	33.3	0.4
	7	2.087	1.2%	0.399	2.8%	1369.7	0.5%	0.19	30.7	0.72	42.6	0.5
									37.7 ± 3.3 Ma		**37.7 ± 6.5 Ma**	
G_12	2	0.604	1.2%	0.125	8.2%	414.6	0.5%	0.21	15.9	0.66	24.1	0.3
	3	0.817	1.2%	0.180	5.8%	437.5	0.5%	0.22	16.3	0.68	23.9	0.3
	4	0.668	1.2%	0.218	4.2%	199.8	0.5%	0.33	15.0	0.73	20.6	0.3
	5	1.416	1.1%	0.161	5.1%	318.5	0.5%	0.11	12.4	0.74	16.7	0.2
									21.1 ± 1.8 Ma		**21.1 ± 3.5 Ma**	
G_13	5	5.586	1.3%	0.191	4.4%	1216.8	0.5%	0.03	14.9	0.75	19.8	0.3
	7	8.858	2.2%	0.933	2.4%	1345.7	0.5%	0.11	24.6	0.81	30.4	0.7
	2	0.775	1.2%	0.191	5.5%	350.3	0.5%	0.25	10.9	0.65	16.8	0.2
	3	2.041	1.2%	0.271	3.9%	336.4	0.5%	0.13	15.6	0.79	19.8	0.2
	4	7.490	1.1%	0.467	2.6%	923.9	0.5%	0.06	24.2	0.83	29.2	0.4
									22.7 ± 2.6 Ma		**22.6 ± 6.1 Ma**	

[a]^{238}U: mass of ^{238}U; ^{232}Th: mass of ^{232}Th; ^{4}He: ^{4}He volume per nano cm^3 STP; Th/U: ^{232}Th to ^{238}U factor; F_T, alpha recoil correction factor after *Farley et al.* [1996]; Corrected age (Ma): corrected He age; ±1σ: sigma standard deviation of corrected age. Italics, average age of sample and ±1σ standard deviation based on central age algorithm [*Vermeesch*, 2010]. Bold, average age of sample and ±1σ standard deviation based on geometric average.

(apatite) and at ~1200°C for 20 min (zircon) [*Foeken et al.*, 2006]. Helium content was measured using a Hiden HAL3F quadrupole mass spectrometer. Apatite-bearing packets were then removed from the He extraction line, spiked with ^{235}U and ^{230}Th in 5% nitric acid and left at 80°C for 48 h in sealed Teflon beakers. Zircon crystals were carefully removed from the foils before being dissolved in 49% HF at 250°C for 48 h in a Parr bomb [*Dobson et al.*, 2008]. ^{238}U, ^{235}U, and ^{232}Th contents were determined via isotope dilution using a Plasmaquad PQ2.5 ICPMS [*Balestrieri et al.*, 2005]. Durango apatite and Fish Canyon Tuff zircon were used as mineral standards. The AHe and ZHe ages were calculated according to established procedures [*Meesters and Dunai*, 2005; *Vermeesch*, 2010], and the ages were corrected for alpha recoil [*Farley et al.*, 1996; *Ketcham*, 2009].

For the AFT analysis, polished apatite crystals were etched at 20°C in a 5.5 M HNO_3 solution for 20 s [*Donelick et al.*, 1999; *Ketcham*, 2005]. ^{238}U concentrations were determined using the external detector method [*Gleadow and Lovering*, 1977]; samples were irradiated at the Garching nuclear reactor, including a CN5 glass dosimeter. The apatite fission track ages were calculated using a zeta value of 368 ± 8 [*Hurford and Green*, 1983]. Fission tracks were counted and measured under a Carl Zeiss Axioplan microscope at X1250 magnification. Average etch pit diameter of fission tracks (Dpar) measurements were calibrated against the Durango apatite standard (300 measurements from an interlaboratory Durango thin section; average Dpar: 1.81 ± 0.1) [*Carlson et al.*, 1999]. Horizontal, confined track lengths could be measured only for two samples; the lengths are *c* axis corrected

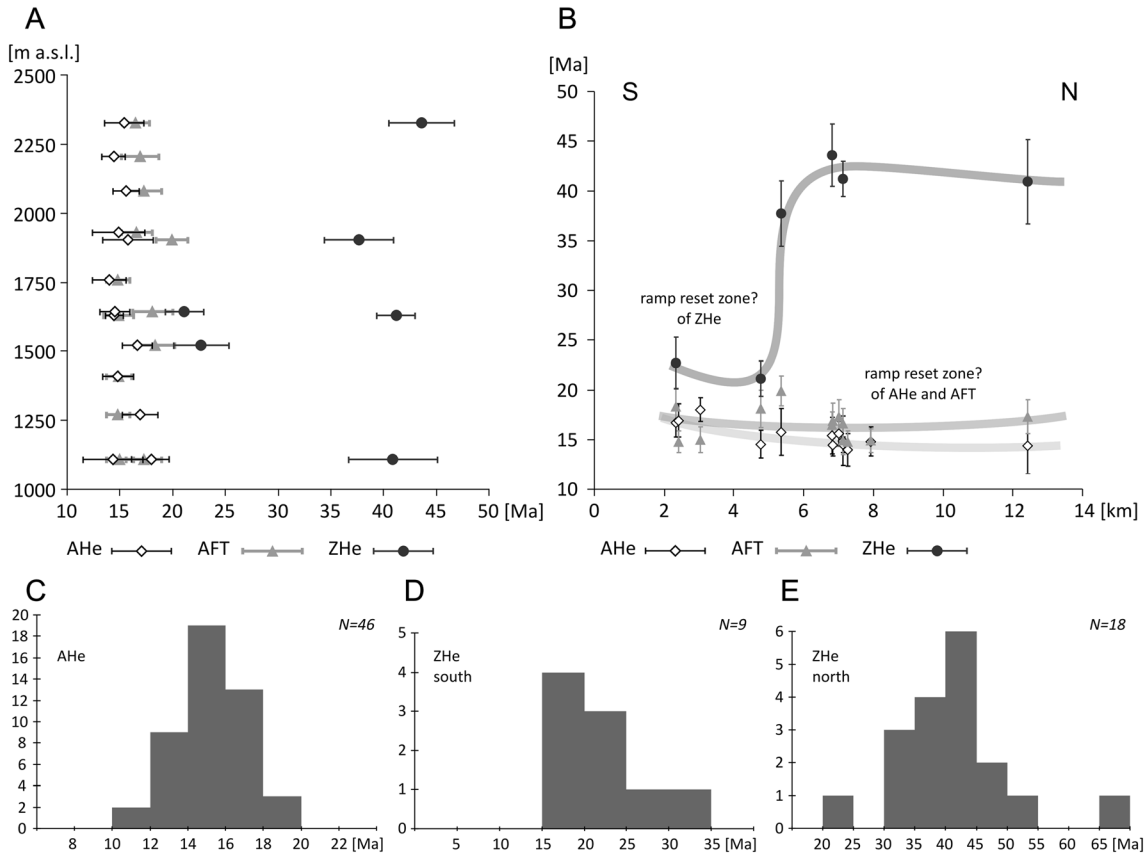

Figure 4. Plots of the thermochronological data, 1 sigma error bars for central ages are shown; age distribution for single-grain ages of the AHe and two populations of the ZHe. (a) Thermochronological age versus vertical position above sea level. (b) Distance from the sub-Tatric fault versus thermochronological age of samples. (c–e) Histograms of the single-grain ages distribution for the: AHe; ZHe in the southern part of the sampled area; ZHe in the northern part of the sampled area. N, number of ages.

[*Carlson et al.*, 1999]. Fission track ages were calculated using Trackkey 4.2 software [*Dunkl*, 2002]. Thermal histories were derived from the HeFTy software, using the annealing algorithm developed by *Ketcham et al.* [2007]. The He data were modeled using the model parameters of *Flowers et al.* [2009] (Activation Energy 29.23 kcal/mol and D_o 0.6071 cm^2/s), as used in the HeFTy software [*Ketcham*, 2009]. The corrected ages are obtained using the alpha correction of *Ketcham* [2009].

4. Results

The data are shown in Tables 1–3 and Figures 3 and 4. We measured three to five single crystal apatite (U + Th)/He ages (AHe) per sample. A total of 53 single crystals were dated (Table 1). Analytical uncertainties on individual age determinations are typically ~5%. Six single ages were rejected because they were significantly older than the AFT age. One datum was rejected because the age was significantly younger than all other ages for the data set (Table 1). More than 85% of age determinations were used in the thermal model. In eight cases the standard deviation for each sample is within 10% of the geometric mean sample age and less than 20% in the other five cases. Average AHe ages vary from ~18 Ma (G15) to ~14 Ma (G05), with 10 of the 13 samples yielding average ages from 15.8 ± 2.4 Ma to 14.0 ± 1.6 Ma. There is no resolvable AHe age change with altitude from the ~1 km subvertical profile from the Morskie Oko lake area and no age-elevation relationship for the whole data set (Figures 3c, 3d, and 4a). There is no clear relation between age and position along the N-S profile through the Tatry, except the ages along sub-Tatric fault being slightly older (Figure 4b). If treated as a single population, all 46 crystals yield ages of 15.2 ± 1.8 Ma with a unimodal and symmetric age distribution (Figure 4c).

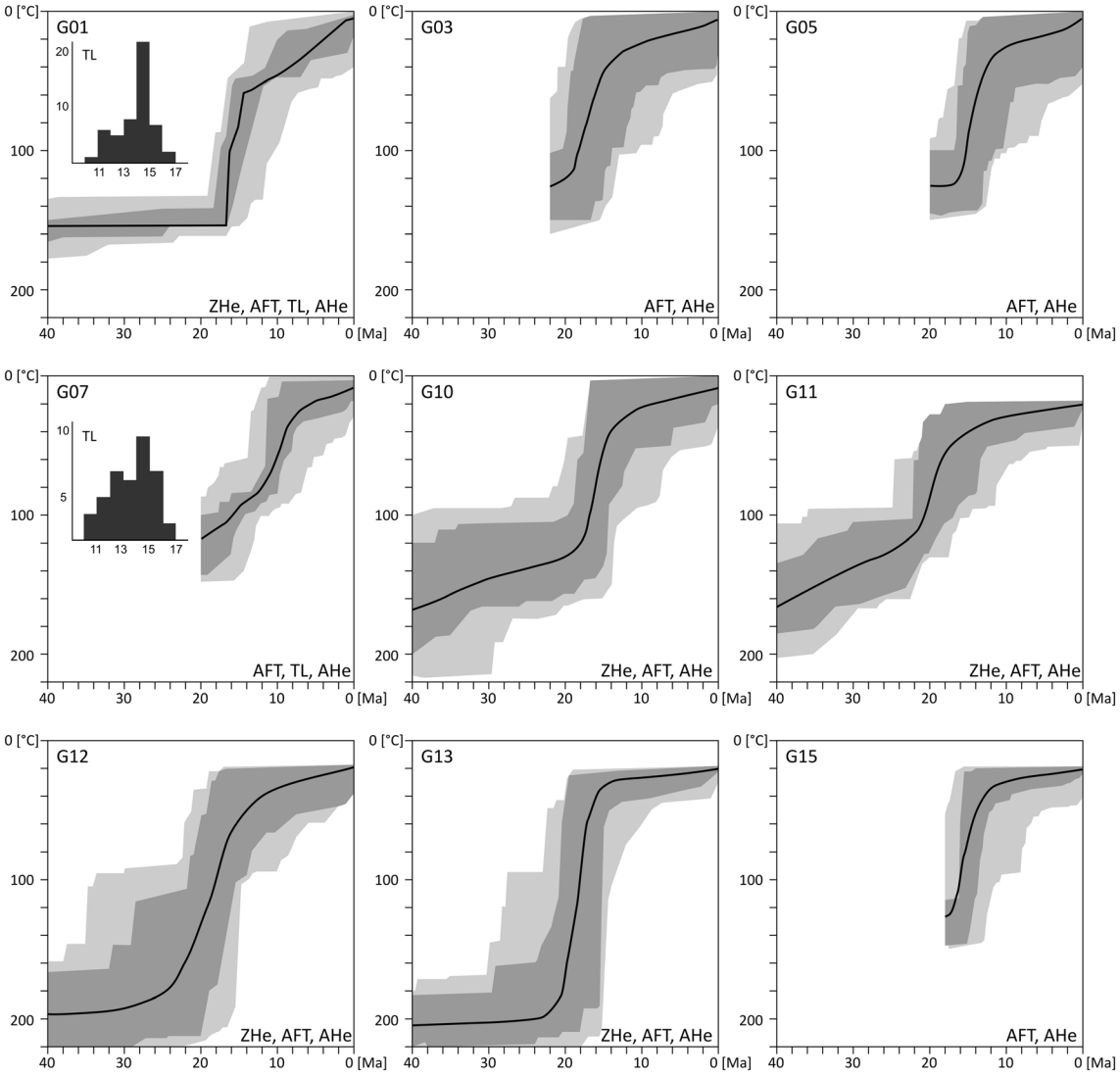

Figure 5. Thermal modeling results of ZHe, AFT, and AHe data for the selected samples displayed as a time-temperature chart. Modeled in HeFTy program [*Ketcham*, 2005]. The best fit is shown as a black line, light gray and dark gray areas show acceptable and good fit, respectively. The models where limited to the temperature of ~120°C for the samples where ZHe data were not available. No geological constraints were used as the different possible tectonic scenarios are being tested by the models. Data sets used for the modeling of samples are given; TL, track length (microns) distribution.

The apatite fission track (AFT) single crystal ages pass the chi-square test in 12 of 13 samples, and therefore, they can be considered as belonging to the same population. Ages vary from ~20 Ma (G11) to ~15 Ma (G05) but 10 out of 13 samples yield average ages between 17.3 ± 1.7 to 14.8 ± 1.1 Ma (Table 2). There is no clear correlation between AFT age and sample location within the massif, but ages tend to be older in the southern part of the N-S horizontal profile (Figures 3 and 4). The four topmost samples of the Morskie Oko profile have ages between 17.3 ± 1.7 and 16.5 ± 1.3 Ma. The three lowermost samples yield ages from 14.9 ± 1.4 to 14.8 ± 1.1 Ma. Dpar values vary from 1.55 to 1.96 μm, with an average for the whole sample set of 1.81 μm ± 0.21 μm ($n = 243$). The Dpar values indicate an F-rich, Durango-like chemical composition of the analyzed apatites, suggesting that complete annealing might have occurred at 110–100°C [e.g., *Carlson et al*., 1999]. The young AFT ages and the low ^{238}U concentrations allowed for a statistically significant number of confined, horizontal tracks to be measured in only two samples (G01 and G07, the top and bottom of the Morskie Oko profile). The track length distribution in both samples is unimodal with mean track lengths of 13.9 μm and 13.3 μm (Figure 5).

In all samples, the AFT ages are older or identical to the AHe ages at 2σ level. The age difference is up to 4.1 Myr (G11) with an average of 1.2 ± 3.1 Myr. The absence of a clear age-elevation relationship in the Morskie Oko profile is consistent with rapid cooling through the FT partial annealing zone (110–60°C) [*Reiners and Brandon*, 2006] (Figures 3 and 4; Tables 1 and 2).

Six samples from the N-S profile were chosen for zircon (U + Th)/He (ZHe) analysis. A total of 27 single grains were dated, from two to nine per sample (Table 3). Analytical uncertainties on individual age determinations are typically less than 2%. Age reproducibility of replicates vary from sample to sample (Table 3). The mean age was calculated by using both the geometric average and central age algorithm [*Vermeesch*, 2010]. Two groups of ages can be distinguished: older ages in the north and central part of the analyzed portion of the Tatry massif and younger in the southern part (Figures 3 and 4). Both groups of single grain ZHe ages show unimodal age distributions (Figures 4d and 4e). Four samples from the northern and central part of the profile yield central ages from 43.6 ± 3.1 Ma (G01) to 37.7 ± 3.3 Ma (G11). Ages from nine single-grain aliquots from the northernmost granite sample (G10) vary from 69.0 ± 0.8 Ma to 23.4 ± 0.4 Ma, with six in range 33–48 Ma. In the southern part of the massif close to the sub-Tatric fault, ZHe ages are around 22 Ma. Two samples that generated nine single-grain aliquots yield central ages of 21.1 ± 1.8 Ma (G12) and 22.7 ± 2.6 Ma (G13) (Table 3).

5. Discussion

5.1. Miocene Cooling History of the Tatry

The AHe and AFT data indicate that the analyzed portion of the Tatry massif cooled during Miocene times (Figures 3 and 4). Thermal history modeling was performed on the samples for which more than one data set was available (AFT age and track length distribution and/or AHe and/or ZHe ages) (Figure 5). Almost all thermal histories show a rapid cooling event between 20 and 14 Ma from at least 100°C to 40°C or less, at a minimum cooling rate of 10°C/Myr (Figure 5). This corresponds to minimum denudation rates of 0.4–0.6 km/Myr for a geothermal gradient of 20–25°C/km. This gradient is considered here as representative of the fore-arc area during subduction and collision [*Dumitru*, 1991], although an elevated geothermal gradient in the Tatry area has also been proposed [*Danišík et al*., 2012; *Anczkiewicz et al*., 2013]. The maximum cooling rate during large portions of this period might have exceeded 20°C/Myr representing denudation rates >1 km/Myr (Figure 5). Since 14 Ma, the rate of cooling appears to have slowed to less than 5°C/Myr. For the two samples at the bottom of the vertical profile (G05, G07) a modeled change in the cooling rate appears at ~10 Ma.

The spatial distribution of the AHe and AFT ages suggests that there is no clear difference in the cooling history from ~100°C between samples. The southern margin of the Tatry might have experienced cooling slightly earlier than the rest of the massif. The lowermost part of the Morskie Oko subvertical profile might have cooled below the relevant closure temperatures later than the higher samples. However, both these interpretations are indistinguishable at the 2σ uncertainty level (Figures 3 and 4).

The ZHe ages from the southern margin of the massif record the exhumation rocks that cooled through ~180°C at ~22 Ma (Figures 3 and 4). By including the ZHe data in the thermal history modeling, the Miocene average cooling rates are estimated at ~20°C/Myr from 22 to 14 Ma (Figure 5). For a geothermal gradient of 20–25°C/km this corresponds to erosion of 5.5 to 7 km during the Miocene and 9 to 7 km since ~22 Ma. This is a greater amount than for the other massifs in the CWC where the total exhumation for the same period of time did not exceed 4–5 km [*Danišík et al*., 2012]. An elevated geothermal gradient during the proposed "mid-Miocene thermal event" (18–11 Ma) [*Danišík et al*., 2012] means that the amount of eroded Tatry calculated above should be considered a maximum. The results imply that the pulse of Miocene rapid cooling (exhumation) started earlier than 22 Ma and is approximately synchronous with the cessation of sedimentation in the CCPB [*Gedl*, 2000; *Soták et al*., 2001; *Garecka*, 2005]

The Paleogene ZHe ages imply that the northern part of the Tatry experienced significantly less Miocene cooling and denudation than the southern edge of the massif (Figures 1 and 3). Depending on the geothermal gradient, the minimum difference in Miocene denudation between the northernmost and southernmost sampled interval is estimated to be 3 to 4 km (Figure 6).

The results presented here enable better constraints on the timing of rapid denudation and cooling, and identify the early and mid-Miocene (22–14 Ma) as a key period in the history of the sampled portion of the

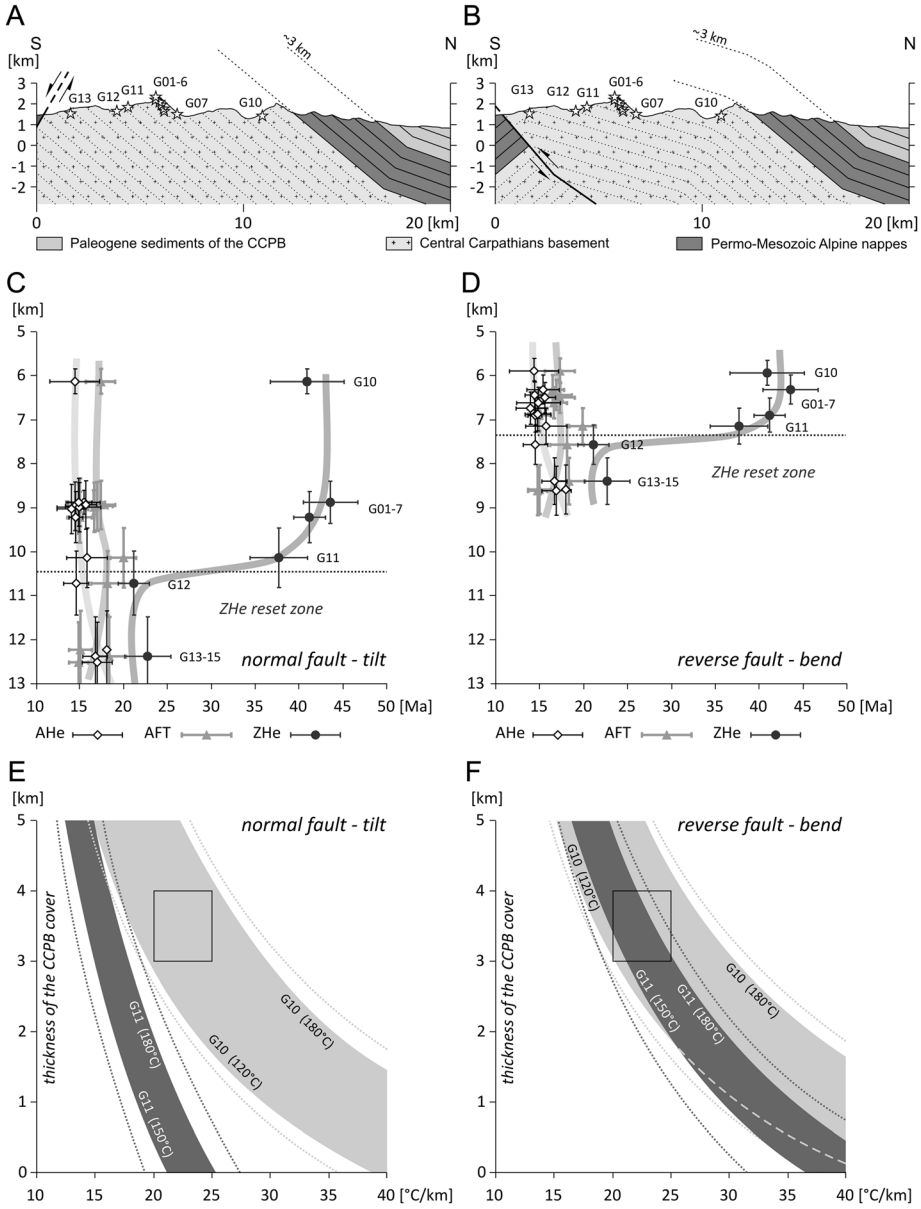

Figure 6. Reconstruction of the early Miocene thermal histories of the samples based on the two main tectonics model of the Tatry (see text for more explanations). (a) Schematic N-S cross section through the Tatry in the sampled area based on the normal fault/tilt block model (3). (b) Schematic N-S cross section through the Tatry in the sampled area based on the reverse fault-/fault-related-fold model (4). (c) Thermochronological age of samples versus the hypothetical vertical position in the profile inferred for the tilt model (3), assuming block rotation of the Tatry crystalline core, 3 km of the CCPB overburden, and normal displacement of the south dipping sub-Tatric fault. See Figure 2d. (d) Thermochronological age of samples versus the hypothetical vertical position in the profile inferred for the fault-related-fold model (4), assuming internal bending of the Tatry crystalline core toward the sub-Tatric fault ("Tatry anticline"), 3 km of the CCPB overburden and reverse displacement of the north dipping sub-Tatric fault. See Figure 2c. (e) Early Miocene palaeothermal gradient versus thickness of Central Carpathian Paleogene Basin sediments cover of the Tatry for the normal fault/tilt block model. Light gray and dark gray areas show the gradient/overburden pairs that meet temperature requirements for G10 and G11 samples, respectively. Dotted lines show uncertainty of the burial estimation. Almost no possible pairs of the gradient and the cover values meet the temperature constraints of the G10 and G11 samples at the same time. Black rectangle shows the range of the most probable gradient and cover values. (f) Early Miocene paleothermal gradient versus thickness of Central Carpathian Paleogene basin sediments cover of the Tatry for the reverse fault-/fault-related-fold model. Light gray and dark gray areas show the gradient/overburden pairs that meet temperature requirements for G10 and G11 samples, respectively. Dotted lines show uncertainty of the burial estimation. Most of the possible pairs of the gradient and the cover values meet the temperature constraints of both samples at the same time. Black rectangle shows the range of the most probable gradient and cover values.

massif. The most recent AFT data from the eastern portion of the Tatry [*Králiková et al*., 2014a] show that the rapid cooling episode might extend to ~10 Ma. These findings suggest that there might be a W-E difference in the mid-Miocene cooling history of the Tatry. The sections of the massif close to the eastern bounding strike-slip fault was still rapidly exhumed while the exhumation in the central part had already slowed [*Král'*, 1977; *Králiková et al*., 2014a].

5.2. Paleogene Thermal History of the Tatry

The first transgression of the Central Carpathian Paleogene Basin sediments onto the pre-Cenozoic basement in the Tatry area occurred at ~42–39 Ma and is clearly recorded by the occurrence of Paleogene conglomerates and shallow marine limestones [*Bartholdy et al*., 1999]. The 12 from 18 single-grain ZHe ages from the northern and central parts of the Tatry that are in range of 37 to 48 Ma might suggest Paleogene cooling after Alpine collision and immediately prior to the subsidence of the CCPB (Figures 3 and 4). This hypothesis is supported by the geological evidences; the recoded ages cannot prove the cooling event by themselves. This hypothetical Eocene cooling may have been related to extension that was responsible for the formation of the fore-arc basin. The hypothesis is consistent with the early tectonic history of the CCPB proposed by *Kázmér et al*. [2003]. Also, it is consistent with structural observations of synsedimentary faults in the CCPB close to the Tatry [*Tomaszczyk et al*., 2009; *Dąbrowska and Jurewicz*, 2013].

Eocene ZHe ages in the northern part of the granitic massif (sample G10) indicate that the stack of Mesozoic nappes formed during Alpine thickening had an original thickness of ~6 km or more, when a thermal gradient ~30°C/km or lower is assumed. The spread of single-grain ZHe ages for the G10 sample indicates that the Mesozoic burial only partially resets some of the zircon grains at that time (Table 3). Alternative, more complex, thermal histories are possible from these data, but they are difficult to reconcile with the regional geology.

The pre-Miocene thermal history is recorded in most of the ZHe ages, despite heating by burial under the CCPB sediments, but no AFT data record Paleogene cooling (Figure 3). These data place limits on the thickness of CCPB sedimentary cover of the Tatry. Clearly it was thin enough to allow preservation of the pre-Miocene ZHe ages but thick enough to reset the AFT system in all samples (Figure 4b). The most reliable estimate of the thickness of the CCPB sedimentary cover can be made for the northernmost part of the sampled granite represented by sample G10 (Figure 3). As the distance of sample G10 from the Mesozoic nappes is relatively small, the uncertainty of the burial estimation caused by the unknown internal structure of the Tatry granitic core is negligible (Figures 6a and 6b). Regardless of the tectonic model of the Tatry exhumation, at the moment of the CCPB transgression, sample G10 was buried beneath ~1 km of granite and ~2 km of Mesozoic nappes [*Nemčok et al*., 1994]. This corresponds to temperatures ~60–75°C, taking into account typical geothermal gradient of 20–25°C/km. In order to fully reset the AFT thermochronometer without resetting ZHe, additional heating of 50°C to 100°C is needed. This equates to 2 to 4 km of the Central Carpathian Paleogene Basin cover (Figure 6). The total current thickness of the CCPB in the Podhale syncline north of the Tatry is ~3.5 km [*Ludwiniak*, 2010]. Therefore, the new low-temperature thermochronological results favor the Tatry being fully covered by the CCPB sediments in the late Paleogene [*Králiková et al*., 2014a].

5.3. Implications for Structural Models for the Formation of the Tatry

Four interpretations for the structural emplacement of the Tatry Mountains are tested here and are illustrated in Figure 2. These models predict contrasting cooling histories for the Tatry:

1. Inherited Cretaceous-Palaeogene Alpine deformation with minor Neogene rejuvenation (Figure 2a). Although there is an apparent pattern of burial and exhumation through the Central Western Carpathians from south to north [*Kováč et al*., 1994; *Plašienka et al*., 2007; *Danišík et al*., 2010] and most of the AFT studies in the Tatry points to 20–10 Ma as a key period of exhumation, this model cannot be simply ruled out. It is supported by the AFT ages of >30 Ma from the western and northern part of the Tatry [*Burchart*, 1972; *Anczkiewicz et al*., 2005] and ~75 Ma ZFT ages from SE part of the massif [*Králiková et al*., 2014a]. In this case the Tatry exhumation would be more similar to the Nízke Tatry massif [*Danišík et al*., 2011] than the Malá Fatra (west of the Tatry) and the Branisko mountains (east of the Tatry) where Neogene cooling ages of 14 to 10 Ma and 20 Ma to 11 Ma, respectively, were identified (Figure 1c) [*Danišík et al*., 2010, 2012].
2. Late Eocene-early Oligocene strike-slip faulting that caused the transpressional uplift and exhumation in the Tatry synchronous with the transtensional development of the CCPB that continued into the Miocene (Figure 2b). This model is based on the Paleogene fault activity dated in the Tatry by

Kohút and Sherlock [2003] supported by the interpretation of the AFT ages. In this model the wide range of the AFT ages in the Tatry is interpreted as a result of continuous process of cooling and exhumation from the Eocene (~40 Ma) to Miocene and even Pliocene times [*Baumgart-Kotarba and Král*, 2002].

3. Extensional footwall uplift during Miocene/Pliocene (Figure 2c). This model is based on the hypothesis that the sub-Tatric fault is a south dipping normal fault [e.g., *Hrušecký et al*., 2002; *Jurewicz*, 2005]. It is supported by the youngest (<12 Ma) AFT ages noted in the Tatry [e.g., *Burchart*, 1972; *Anczkiewicz et al*., 2005], especially along the sub-Tatric fault [*Baumgart-Kotarba and Král*, 2002]. In this interpretation the major exhumation in the Tatry coincided with the postorogenic extension episode in the region [*Nemčok et al*., 2006a; *Tokarski et al*., 2012].
4. Backthrusting during Carpathian orogenesis in early-middle Miocene (Figure 2d). This model is based on the hypothesis that the sub-Tatric fault is a north dipping reverse fault [e.g., *Sperner*, 1996; *Sperner et al*., 2002]. It is supported by the basic geometric restoration of the sub-Tatric fault [*Plašienka et al*., 2001] and by the AFT ages of ~20 to ~15 Ma in the Tatry. In this model the major episode of the cooling and exhumation of the Tatry occurred during the contraction stage related to the Carpathian orogenesis.

Model 1 predicts that the main stage of the Tatry exhumation is similar to the exhumation of the Nízke Tatry (Figure 2a). Eocene cooling ages that are recorded in the ZHe thermochronometer in the northern part of the Tatry are partially similar to Eocene ZHe ages of the Nízke Tatry [*Danišík et al*., 2010]. On the other hand, in the Tatry we have not recorded any Paleogene AFT ages, not even in the northernmost sample G10 close to the Mesozoic cover. All AFT data along with AHe and even part of the ZHe ages from the south of the study area point to a distinct Miocene exhumation period. These results indicate that the hypothesis of Cretaceous-Paleogene final emplacement of the Tatry massif can be ruled out. Taking into account ~7 km of Miocene exhumation, it must be noted that the tectonic evolution of the Tatry has been somewhat different not only from one of the Nízke Tatry but also from the Malá Fatra (west of the Tatry) and the Branisko mountains (east of the Tatry) [*Danišík et al*., 2010, 2012].

Model 2 implies that the exhumation of the Tatry was synchronous with sedimentation in the CCPB from 40 to 23 Ma (Figure 2b). This is also inconsistent with the thermal histories derived here. In order to completely reset the AFT ages in the northern part of the granite and ZHe ages in the southern part, CCPB sediments need to have covered the massif, unless gradients were above 40°C/km (Figure 6). The ZHe ages indicate exhumation prior to sedimentation in the CCPB or after sedimentation. What is even more important is that none of the AFT and AHe data presented here record exhumation during Paleogene sedimentation (Figure 3). The ~30 Ma AFT results are characteristic of the western and northwestern area of the Tatry as suggested by *Burchart* [1972] and *Anczkiewicz et al*. [2005]. These AFT data, however, could also be interpreted as an effect of partial resetting under insufficient Paleogene cover, rather then cooling and exhumation [*Środoń et al*., 2006]. Our thermochronometric data indicate that the CCPB caused the burial and heating of the Tatry area and that exhumation was not continuous from the early Paleogene to the Miocene/Pliocene times, as predicted by model 2. If this is the case, the Paleogene fault activity in the Tatry area recorded by *Kohút and Sherlock* [2003] might be linked to the development of the CCPB rather than continuous exhumation of the Tatry.

Both the remaining tectonic models (Models 3 and 4, Figures 2a, 2b; 6a, and 6b) imply that exhumation took place in the Neogene and are in general agreement with the results presented here. Exhumation of the Tatry block has been explained either by rotation and uplift due to normal faulting (model 3) [*Jurewicz*, 2005] or a fault-related-fold mechanism along a back thrust (model 4) [*Plašienka et al*., 2001]. Model 3 links middle and late Miocene exhumation of the Tatry with the postcollisonal phase of the Outer Carpathians and postrifting phase of the Pannonian basin in late Miocene (16–5.3 Ma) or even Pliocene times (5.3–1.8 Ma) [*Baumgart-Kotarba and Král*, 2002; *Tokarski et al*., 2012]. Model 4 suggests exhumation synchronous with shortening in the Outer Carpathians and syn-rift phase in the Pannonian basin [*Sperner et al*., 2002] in the early and middle Miocene (~23–12 Ma). The timing of the main exhumation event presented in this study (~22–14 Ma) strongly favors model 4. However, the cooling ages cannot by themselves completely rule out the alternative mechanism. Discriminating between these models is only possible by combining the spatial distribution of cooling ages with structural, tectonic, and stratigraphic information.

5.4. Extensional Footwall Exhumation Model (Model 3)

The main phase of exhumation of the Tatry range recorded by data presented in this study is similar to the time of exhumation of the Alcapa block and the onset of the rifting processes associated with the formation

of the Pannonian basin ~100 km to the south of the Tatry [*Royden et al*., 1983; *Horváth*, 1993]. However, the spatial distributions of cooling ages cannot be easily explained using an extensional footwall exhumation (model 3). The age distribution pattern in the footwall of a normal fault should be characterized by younging of the thermochronological ages toward the fault. For example, the Wassuk Range and Grey Hills in western Nevada represent a Miocene tilted fault block that displays ~60° of footwall rotation and exposure of preextensional paleodepths of up to ~8.5 km [*Stockli*, 2005]. The distribution of thermochronometric ages through the tilted footwall block show ages becoming younger toward the main fault zone where the deepest part of the profile is exposed. This pattern is especially clear for the AHe and AFT thermochronometers [*Stockli*, 2005] but is not recorded by the spatial distribution of thermochronology ages in the Tatry massif presented here (Figures 3, 4b, and 6b).

In order to test the tilted footwall block model, we have reconstructed the Miocene maximum burial of the samples taking into account a 35–45° northward tilt of the Tatry block and ~3 km of CCPB cover (Figure 6a). The same reconstruction was made for the fault-related-fold model (Figure 6b). Results are plotted against thermochronological age [*Stockli*, 2005] (Figures 6c and 6d). These reconstructions show that samples G10 and G11 are crucial for placing constraints on the early Miocene thermal history of the Tatry. Both samples record the same Miocene AFT ages and similar Paleogene ZHe ages despite being placed ~6.5 km from each other (Figure 3). For G10, two grains of nine show older ZHe ages that might suggest only partial resetting under the Mesozoic cover of nappes and for G11 two grains are younger showing tendency to being reset by the early Miocene burial (Table 3). The thermochronological results might be transferred to the early Miocene temperatures of 120–180°C for the G10 and 150–180°C for sample G11. For the tilted footwall block model the difference in predicted burial between these two samples is 3 to 5 km; this conclusion suggests that they would not end up with similar thermal histories and hence challenges the tilted footwall block interpretation. Temperature constraints for these samples cannot be met for almost all combinations of the palaeothermal gradient and the CCPB overburden except unrealistically low gradient and high overburden (Figure 6e). In the case of the reverse fault model the reconstructed vertical difference between samples G10 and G11 is 1–1.8 km, and the temperature constraints can be met over a wide range of gradients and CCPB cover thicknesses (Figure 6f).

An additional challenge for the normal fault model is that a displacement of 13–15 km is required to balance the cross section [*Plašienka et al*., 2001]. For a fault of ~50 km length (Figure 1) this is uncommon even in the Basin and Range province where extreme extension has occurred [*Byrd et al*., 1994]. Numerous tectonic studies and paleostress reconstructions show that in the northern part of the CWC range compression and contraction dominated until the end of middle Miocene, with the change to extension occurring after ~10 Ma [*Nemčok et al*., 2006a, and references therein]. All these arguments, combined with the observation that the exhumation of the Tatry was synchronous with the regional shortening in the area, suggest that the interpretation of exhumation in the Tatry in terms of only rotation and uplift of a normal fault block is difficult to reconcile with the data.

5.5. Reverse Fault Exhumation Model (Model 4)

At the same time as rifting in the Pannonian region south of the CWC, contraction and thrusting were at their peak in the Outer Carpathian thrust wedge, ~20–100 km north of the Tatry massif [*Andreucci et al*., 2013]. Nappe formation processes ceased in this sector of the Outer Carpathians at ~13.6 Ma [*Nemčok et al*., 2006a, 2006b] at the same time as exhumation in the Tatry decelerated (Figures 3 and 5). The Podhale syncline is located between the Outer Carpathians and the Tatry and represents a relic of the Central Carpathian Paleogene Basin (Figure 1). This structure was deformed after cessation of sedimentation in the CCPB ~23 Ma [*Gedl*, 2000; *Garecka*, 2005], but before the development of the unconformably overlying Orava-Nowy Targ basin at ~14 to 12 Ma [*Tokarski et al*., 2012; *Łoziński et al*., 2014], synchronously with the main stage of the Tatry exhumation. The structural data indicate N-S horizontal compression in forming the syncline and its related tectonic mesostructures [*Mastella*, 1975; *Ludwiniak*, 2010].

The tectonic model of the Tatry exhumation proposed by *Sperner* [1996] and *Sperner et al*. [2002] suggests that the Tatry block was exhumed in the hanging wall of a thrust fault localized between two major strike-slip fault zones that cut the Mesozoic basement of the CCPB (Figures 1d and 2c). In this interpretation the sub-Tatric fault might be considered as a result of the deformation in the transpressive overlap between two sinistral faults [*Kim et al*., 2004; *Oglesby*, 2005]. The interpretation was modified by *Plašienka et al*. [2001]

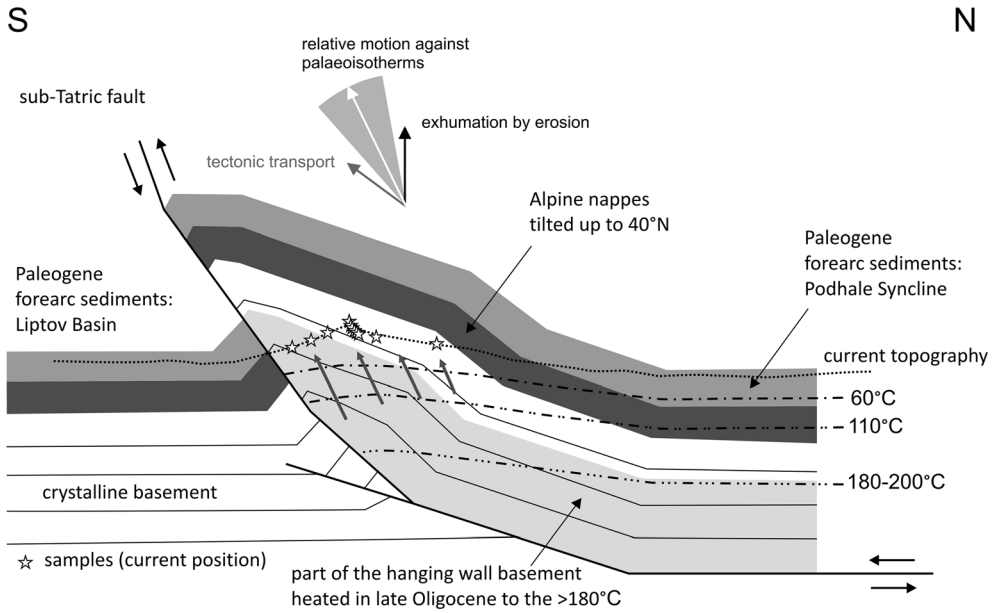

Figure 7. Schematic cross section through the Tatry with the proposed scenario of the general thermal history of the samples. White stars, current position of sampled sites. Grey arrows show the net direction of the samples movement versus paleo-isotherms being the result of erosion and tectonic transport along the thrust during the main stage of the exhumation. Light gray area, current position of the part of the hanging wall basement heated in late Oligocene to the temperatures >180°C.

who proposed a fault-related-fold structure for the development of the "Tatry anticline" that grew simultaneously with the Podhale syncline (Figure 6c). This model reduces the total fault slip needed to balance the cross section from the rather extreme values of ~18 km to a more reasonable ~8 km [*Plašienka et al.*, 2001; *Sperner et al.*, 2002]. This value agrees with the 9 to 7 km of exhumation during the last ~22 Ma close to the sub-Tatric fault presented in this paper (Figures 6d and 6f).

A further test of the fault-related-fold model comes from the spatial distribution of ZHe, AFT, and AHe ages throughout the Tatry massif. The transport over a back thrust, as hypothesized in the model, would cause the growth of the "Tatry anticline" and block rotation of the hanging wall at the base of the ramp [cf. *Narr and Suppe*, 1994]. That would produce a zone of similar thermochronological ages across the massif, in the so called "ramp reset zone" as a "bottom" part of a U-shaped age distribution [*Lock and Willett*, 2008]. Such a distribution is typically built up from the "old" ages in the footwall near the thrust, "young" and uniform reset ages across the massif and "old" ages away from the thrust in the back limb of the fold. As shown by a series of theoretical thermal models by *Lock and Willett* [2008], the "ramp reset zone" is narrower for high closure temperature thermochronometers. This means that while the AHe and AFT ages are still uniform in the "ramp reset zone," the ZHe age distribution might show older, preserved cooling ages. The transition between zones of young and old cooling ages is sharp for single-fault models that might be comparable to the sub-Tatric fault. Also, for a large range of model parameters such as fault dip, depth to the base of the ramp, or fault slip rate, the difference between AHe and AFT ages is very small, typically less then 2 Ma. All of these features are reflected in the ZHe, AFT, and AHe ages distribution in the part of the Tatry analyzed here (Figures 3, 4b, 6b, and 6d). The data presented here do not allow us to speculate whether the sub-Tatric fault and related "Tatry anticline" formed as a fault-bend-fold or fault-propagation-fold.

Having considered the alternatives between extension and thrusting, we propose that the simplest explanation for the pattern of cooling ages is that of major exhumation of the Tatry due to displacement and exhumation in the hanging wall of a back thrust (Figure 7). The timing, combined with the N-S age distribution and the paleotemperature constraints on single samples need to be met to fit the model. When these are combined with geological evidence such as restrictions on the balancing of the fault displacement or evolution of the CCPB, they all support the back-thrust hypothesis. The Miocene cooling started most probably with the forming of the "Tatry anticline" as a fault-related-fold and progressed with the further development of the back

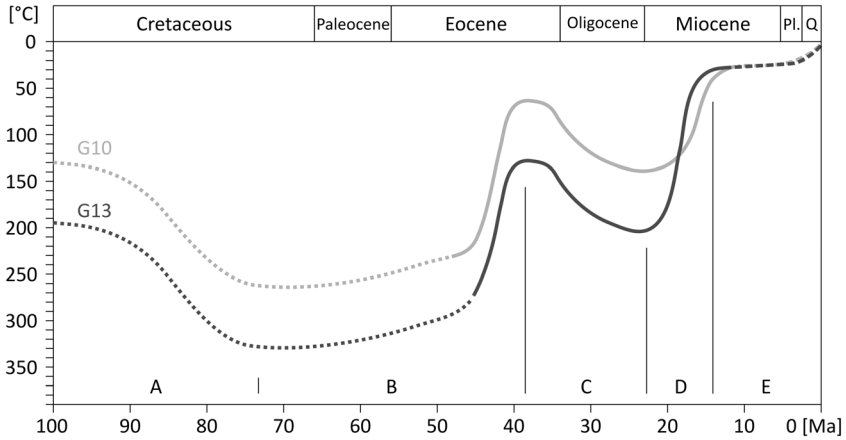

Figure 8. Thermal history of the Tatry granite presented for the northernmost (G10) and southernmost (G13) samples. Solid line, thermal history inferred directly from the cooling ages presented in this study. Dotted line, history based on the *Plašienka et al*. [1997] and ZFT ages of *Králiková et al*. [2014a]. Dashed line, the youngest part of the thermal history. Pl, Pliocene; Q, Quaternary; A, tectonosedimentary burial and heating under the Mesozoic sediments and alpine nappes; B, cooling and exhumation accelerated in the first stages of the fore-arc basin formation; C, burial and heating under CCPB sediments; D, exhumation of the hanging wall ramp of the sub-Tatric fault and related cooling; E, rapid deceleration of exhumation and cooling associated with end of deformation in the Outer Carpathians.

thrust. This back thrust might have formed in the compressional overlap between two major strike-slip faults at the time when horizontal compression was transferred via collision zone from the orogenic wedge of the Outer Carpathians to the edge of the overriding plate (Figure 1c and 2c). However, it cannot be excluded that the sub-Tatric fault and other faults that bound the Tatry massif from west and east were reactivated and achieved important dip-slip normal component of displacement in the late Miocene and Pliocene times [*Sperner et al*., 2002; *Králiková et al*., 2014a].

5.6. Exhumation of the Tatry and Topographic Growth of the Mountains

The low-temperature thermochronology presented here demonstrates that the Tatry massif was rapidly exhumed between 22 and at least 14 Ma, probably along a northward dipping thrust fault (Figure 7). The likely presence of sedimentary rocks from the CCPB covering the Tatry may have favored efficient erosion during the initial stages of exhumation. Factors that may have influenced the decrease in cooling rates (from ~20°C to $<$5°C/Myr) at ~14 Ma include the follwing: the end of the mid-Miocene climate optimum at 14–13.5 Ma and possible related change in weathering rates [*Böhme*, 2003]; the exhumation of the more resistant rocks of the Mesozoic nappes and later Variscan basement; and the transition to a less tectonically active postorogenic phase. How much of the present topography is inherited from the Miocene exhumation event is unknown. A glacial landscape and the widespread presence of conglomeratic alluvial fans and glaciogenic deposits containing granitic clasts from the Tatry massif indicate that Quaternary erosion was important [*Birkenmajer*, 2009]. Such Quaternary exhumation was not big enough to affect the AHe ages, even at the bottom of the sampled valleys. Although the present topographic elevation and relief of the Tatry Mountains (Figure 1b) could be as young as Quaternary [*Králiková et al*., 2014a], the thermochronological ages presented here strongly indicate that the majority of the exhumation occurred in the early and mid-Miocene and that, since then, less than 2–3 km of rocks have been eroded.

5.7. The Tatry as the Boundary Between the Outer Carpathian and Pannonian Systems

Applying three different low-temperature techniques allows us to reconstruct the dynamic thermal history of the Tatry (Figure 8). The history includes tectonosedimentary burial in the Mesozoic followed by the exhumation that was the precursor to the initiation of fore-arc basin formation in the Paleogene [*Plašienka et al*., 1997]. The termination of sedimentation in the fore arc marked the beginning of the Tatry exhumation in the Miocene. This was associated with northward propagation of the Outer Carpathian thrust wedge and development of the sub-Tatric fault as a major retrovergent thrust. The remnant fore-arc basin (the CCPB) was intensively deformed at its northern margin with the Pieniny Klippen Belt [*Soták et al*., 2001; *Ludwiniak*, 2010].

The northward propagation of the Outer Carpathians accompanied by the southward overthrusting of the Tatry records the overall expansion of a doubly vergent west Carpathian thrust wedge. The synchronous expansion of the Outer Carpathian/Tatry thrust wedge with the extension in the Pannonian Basin marks a significant change in the evolution of the system [*Royden et al.*, 1983; *Houseman and Gemmer*, 2007]. The possibility that the sub-Tatric thrust was later reactivated by extensional faulting would fit with models of slab rollback and expansion of back-arc extension; this possibility requires further testing. The shortening on the sub-Tatric fault was laterally accommodated along major strike-slip faults. That enabled the northward extrusion of the Carpathian arc and block rotation in the Outer Carpathians region during Miocene times [e.g., *Konon*, 2001].

6. Conclusions

The combination of new low-temperature thermochronology and geological evidence allows us to reconstruct the tectonic evolution of the Tatry block.

1. The 43.6 ± 3.1 to 40.9 ± 4.2 Ma ZHe central ages might be interpreted to record a phase of Paleogene exhumation in the Tatry that occurred prior to the onset of sedimentation of the CCBP (at 42–39 Ma). Additionally, they suggest that the original cover of the Mesozoic nappes was thick enough to heat almost all the granite in the Tatry area in excess of 180°C.
2. From 40 Ma until ~23 Ma the Tatry were reheated by burial underneath at least ~3 km of sediments in the CCPB.
3. The pre ~21 Ma cooling of the southernmost samples through the zircon He closure temperature is interpreted to have been linked to rotation during transport over a back-thrust ramp developed in the overlap between two major sinistral strike-slip faults. This is associated with termination of sediment accumulation in the CCPB and the onset of deformation of the Podhale syncline.
4. Cooling at ~20°C/Myr resulted in AHe and AFT ages ranging from ~18 to ~14 Ma interpreted as ongoing exhumation of the hanging wall ramp of the sub-Tatric fault.
5. Modeled cooling histories require an abrupt deceleration in cooling after ~14 Ma to rates of <5°C/Myr. This is associated with the end of deformation in the Outer Carpathians and in the Podhale syncline; it is synchronous with the transition of the Pannonian Basin from a syn-rift to a post-rift phase and with termination of N-S compression in the northern part of the Central Western Carpathians.
6. The combination of new thermochronological data with constraints from the regional geology supports an interpretation for the emplacement of the Tatry by upward displacement in the hanging wall of a major back thrust that now forms the sub-Tatric fault. This thrusting pierced through the former fore-arc succession of the CCPB. The timing of shortening is synchronous with formation of the Outer Carpathian orogenic wedge and hence can be seen as the retrovergent thrust bounding the southern margin of the thrust wedge.

Acknowledgments

This work was completed as part of the project "Mechanisms of uplift and erosion in the Carpathian thrust wedge and foreland basin (TopoEurope-ThermoEurope)," jointly funded by the Ministry of Science and Higher Education and by the European Science Foundation. Tatranský Národný Park (Slovakia) and Tatrzański Park Narodowy (Poland) are thanked for approval of rock sampling. Paweł Aleksandrowski (PGI, Wrocław, Poland), Katarzyna Pisaniec (Schlumberger, Gatwick, UK), and Artur Niedzielski are thanked for all the fun and hard work during the field trips and discussions regarding various aspects of tectonic evolution of the Tatry Mountains. Also, Waldemar Śmigielski is thanked for sharing his experience regarding paths in Tatry and help in choosing location for sampling profiles. All participants of the Topo-Europe project are thanked for valuable scientific discussions during workshops and meetings. David Chew and Martin Danišík are thanked for their detailed and constructive comments; their reviews substantially improved a first version of the manuscript. All key data used for this paper are published here in form of figures or tables. Any additional information will be provided by the main author on e-mail request.

References

Anczkiewicz, A. A., M. Zattin, and J. Środoń (2005), Cenozoic uplift of the Tatras and Podhale basin from the perspective of the apatite fission track analyses, *Mineral. Soc. Pol. Spec. Pap.*, *25*, 261–264.

Anczkiewicz, A. A., J. Środoń, and M. Zattin (2013), Thermal history of the Podhale Basin in the internal Western Carpathians from the perspective of apatite fission track analyses, *Geol. Carpath.*, *64*(2), 141–151, doi:10.2478/geoca-2013-0010.

Andreucci, B., A. Castelluccio, L. Jankowski, S. Mazzoli, R. Szaniawski, and M. Zattin (2013), Burial and exhumation history of the Polish Outer Carpathians: Discriminating the role of thrusting and post-thrusting extension, *Tectonophysics*, *608*, 866–883, doi:10.1016/j.tecto.2013.07.030.

Balestrieri, M. L., F. M. Stuart, C. Persano, E. Abbate, and G. Bigazzi (2005), Geomorphic development of the escarpment of the Eritrean margin, southern Red Sea from combined apatite fission-track and (U–Th)/He thermochronometry, *Earth Planet. Sci. Lett.*, *231*, 97–110, doi:10.1016/j.epsl.2004.12.011.

Bartholdy, J., S. M. Bellas, V. Ćosović, P. Fuček, and H. Keupp (1999), Eocene mid-latitude larger foraminifera accumulations: Modelling of the stratigraphic architecture of a fore-arc basin (Podhale Basin, Poland), *Geol. Carpath.*, *50*(6), 435–448.

Baumgart-Kotarba, M., and J. Král (2002), Young tectonic uplift of the Tatra Mts (fission track data and geomorphological arguments), Geologica Carpathica, 53, Special Issue – CD with extended abstracts.

Birkenmajer, K. (2009), Quaternary glacigenic deposits between the Biała Woda and the Filipka valleys, Polish Tatra Mts, in the regional context, *Stud. Geol. Pol.*, *132*, 91–115.

Böhme, M. (2003), Miocene climatic optimum: Evidence from lower vertebrates of central Europe, *Palaeogeogr. Palaeoclimatol. Palaeoecol.*, *195*, 389–401, doi:10.1016/S0031-0182(03)00367-5.

Burchart, J. (1972), Fission track age determinations of accessory apatite from the Tatra Mountains, Poland, *Earth Planet. Sci. Lett.*, *15*, 418–422.

Burda, J., A. Gawęda, and U. Klötzli (2013), U-Pb zircon age of the youngest magmatic activity in the High Tatra granites (Central Western Carpathians), *Geochronometria*, *40*(2), 134–144, doi:10.2478/s13386-013-0106-9.
Byrd, J. O., R. B. Smith, and J. W. Geissman (1994), The Teton fault, Wyoming: Topographic signature, neotectonics, and mechanisms of deformation, *J. Geophys. Res.*, *99*(B10), 20,095–20,122, doi:10.1029/94JB00281.
Carlson, W. D., R. A. Donelick, and R. A. Ketcham (1999), Variability of apatite fission track annealing kinetics: I. Experimental results, *Am. Mineral.*, *84*, 1213–1223.
Csontos, L., and A. Vörös (2004), Mesozoic plate tectonic reconstruction of the Carpathian region, *Palaeogeogr. Palaeoclimatol. Palaeoecol.*, *210*, 1–56, doi:10.1016/j.palaeo.2004.02.033.
Dąbrowska, M., and E. Jurewicz (2013), Character and structural evolution of the Mała Łąka Fault in the Tatra Mts., Carpathians, Poland, *Acta Geol. Pol.*, *63*(1), 137–151, doi:10.2478/agp-2013-0005.
Danišík, M., I. Dunkl, M. Putiš, W. Frisch, and J. Kráľ (2004), Tertiary burial and exhumation history of basement highs along the NW margin of the Pannonian Basin—An apatite fission track study, *Aust. J. Earth Sci.*, *95*(96), 60–70.
Danišík, M., M. Kohút, I. Broska, and W. Frisch (2010), Thermal evolution of the Malá Fatra Mountains (Central Western Carpathians): Insights from zircon and apatite fission track thermochronology, *Geol. Carpath.*, *61*(1), 19–27, doi:10.2478/v10096-009-0041-0.
Danišík, M., J. Kadlec, C. Glotzbach, A. Weisheit, I. Dunkl, M. Kohút, N. J. Evans, M. Orvošová, and B. J. McDonald (2011), Tracing metamorphism, exhumation and topographic evolution in orogenic belts by multiple thermochronology: A case study from the Nízke Tatry Mts., Western Carpathians, *Swiss J. Geosci.*, *104*(2), 285–298, doi:10.1007/s00015-011-0060-6.
Danišík, M., M. Kohut, N. J. Evans, and B. J. McDonald (2012), Eo-Alpine metamorphism and the 'mid-Miocene thermal event' in the Western Carpathians (Slovakia): New evidence from multiple thermochronology, *Geol. Mag.*, *149*(01), 158–171, doi:10.1017/S0016756811000963.
Dobson, K. J., F. M. Stuart, and T. J. Dempster (2008), U and Th zonation in Fish Canyon Tuff zircons: Implications for a zircon (U-Th)/He standard, *Geochim. Cosmochim. Acta*, *72*(19), 4745–4755, doi:10.1016/j.gca.2008.07.015.
Donelick, R. A., R. A. Ketcham, and W. D. Carlson (1999), Variability of apatite fission-track annealing kinetics: II. Crystallographic orientation effects, *Am. Mineral.*, *84*, 1224–1234.
Dumitru, T. A. (1991), Effects of subduction parameters on geothermal gradients in forearcs, with an application to Franciscan subduction in California, *J. Geophys. Res.*, *96*(B1), 621–641, doi:10.1029/90JB01913.
Dunkl, I. (2002), Trackkey: A windows program for calculation and graphical presentation of fission track data, *Comput. Geosci.*, *28*, 3–12, doi:10.1016/S0098-3004(01)00024-3.
Farley, K. A., R. A. Wolf, and L. T. Silver (1996), The effects of long alpha-stopping distances on (U-Th)/He ages, *Geochim. Cosmochim. Acta*, *60*(21), 4223–4229.
Flowers, R. M., R. A. Ketcham, D. L. Shuster, and F. K. Farley (2009), Apatite (U-Th)/He thermochronometry using a radiation damage accumulation and annealing model, *Geochim. Cosmochim. Acta*, *73*(8), 2347–2365, doi:10.1016/j.gca.2009.01.015.
Foeken, J. P. T., F. M. Stuart, C. Persano, K. Dobson, and D. Vilbert (2006), A diode laser system for heating minerals for (U-Th)/He chronometry, *Geochem. Geophys. Geosyst.*, *7*, Q04015, doi:10.1029/2005GC001190.
Foeken, J. P. T., C. Persano, F. M. Stuart, and M. ter Voorde (2007), Role of topography in isotherm perturbation: Apatite (U-Th)/He and fission track results from the Malta tunnel, Tauern Window, Austria, *Tectonics*, *26*, TC3006, doi:10.1029/2006TC002049.
Gągała, Ł., J. Vergés, E. Saura, T. Malata, J.-C. Ringenbach, P. Werner, and P. Krzywiec (2012), Architecture and orogenic evolution of the northeastern Outer Carpathians from cross-section balancing and forward modeling, *Tectonophysics*, *532–535*, 223–241, doi:10.1016/j.tecto.2012.02.014.
Garecka, M. (2005), Calcareous nanoplankton from the Podhale Flysch (Oligocene-Miocene, Inner Carpathians, Poland), *Stud. Geol. Pol.*, *124*, 353–369.
Gedl, P. (2000), Biostratigraphy and palaeoenvironment of the Podhale Palaeogene (Inner Carpathians, Poland) in the light of palynological studies. Part. I [in Polish with English summary], *Stud. Geol. Pol.*, *117*, 69–154.
Gleadow, A. J. W., and J. F. Lovering (1977), Geometry factor for external detectors in fission track dating, *Nucl. Track Detection*, *1*(2), 99–106.
Horváth, F. (1993), Toward a mechanical model for the formation of the Pannonian Basin, in The Origin of Sedimentary Basins: Inferences from Quantitative Modelling and Basin Analysis, papers presented at the ILP Task Force "Origins of Sedimentary Basins" Meeting in Matrahaza (Pannonian Basin, Hungary), 26 September - 2 October 1991, edited by S. Cloetingh et al., pp. 333–357, Tectonophysics, 226(1/4), doi:10.1016/0040-1951(93)90126-5.
Houseman, G. A., and L. Gemmer (2007), Intra-orogenic extension driven by gravitational instability: Carpathian-Pannonian orogeny, *Geology*, *35*(12), 1135–1138, doi:10.1130/G23993A.1.
Hrušecký, I., L. Pospišil, and M. Kohút (2002), Geological interpretation of the reflection seismic profile 753/92, in *Hydrocarbon Potential of the Eastern Slovakian Basin and Adjacent Areas*, edited by I. Hrušecký et al., GSSR, Bratislava.
Hurford, A. J., and P. F. Green (1983), The zeta age calibration of fission-track dating, *Isot. Geosci.*, *1*, 285–317.
Jurewicz, E. (2005), Geodynamic evolution of the Tatra Mts. and the Pieniny Klippen Belt (Western Carpathians): Problems and comments, *Acta Geol. Pol.*, *55*(3), 295–338.
Kázmér, M., I. Dunkl, W. Frisch, J. Kuhlemann, and P. Ozsvárt (2003), The Palaeogene forearc basin of the Eastern Alps and Western Carpathians: Subduction erosion and basin evolution, *J. Geol. Soc. London*, *160*, 413–428, doi:10.1144/0016-764902-041.
Ketcham, R. A. (2005), Forward and inverse modeling of low-temperature thermochronometry data, *Rev. Mineral. Geochem.*, *58*(1), 275–314, doi:10.2138/rmg.2005.58.11.
Ketcham, R. A. (2009), Refinements for alpha stopping distances and FT corrections, OnTrack, the electronic newsletter of the international thermochronology community, 16.
Ketcham, R. A., A. C. Carter, R. A. Donelick, J. Barbarand, and A. J. Hurford (2007), Improved modeling of fission-track annealing in apatite, *Am. Mineral.*, *92*, 799–810, doi:10.2138/am.2007.2281.
Kim, Y. S., D. C. Peacock, and D. J. Sanderson (2004), Fault damage zones, *J. Struct. Geol.*, *26*(3), 503–517, doi:10.1016/j.jsg.2003.08.002.
Kirstein, L. A., H. Sinclair, F. M. Stuart, and K. Dobson (2006), Rapid early Miocene exhumation of the Ladakh batholith, western Himalaya, *Geology*, *34*(12), 1049–1052, doi:10.1130/G22857A.1.
Kohút, M., and S. C. Sherlock (2003), Laser microprobe ^{40}Ar-^{39}Ar analysis of pseudotachylyte and host-rocks from the Tatra Mountains, Slovakia: Evidence for late Palaeogene seismic/tectonic activity, *Terra Nova*, *15*(6), 417–424, doi:10.1046/j.1365-3121.2003.00514.x.
Konon, A. (2001), Tectonics of the Beskid Wyspowy Mountains (Outer Carpathians, Poland), *Geol. Q.*, *45*(2), 179–204.
Kováč, M., J. Král', E. Márton, D. Plašienka, and P. Uher (1994), Alpine uplift history of the Central Western Carpathians: Geochronological, paleomagnetic sedimentary and structural data, *Geol. Carpath.*, *45*, 83–96.
Král', J. (1977), Fission track ages of apatites from some granitoid rocks in West Carpathians, *Geol. Carpath.*, *28*, 269–276.

Králiková, S., R. Vojtko, L. Sliva, J. Minár, B. Fügenschuh, M. Kováč, and J. Hók (2014a), Cretaceous–Quaternary tectonic evolution of the Tatra Mts (Western Carpathians): Constraints from structural, sedimentary, geomorphological, and fission track data, *Geol. Carpath.*, *65*(4), 307–326, doi:10.2478/geoca-2014-0021.

Králiková, S., R. Vojtko, P. Andriessen, M. Kováč, B. Fügenschuh, J. Hók, and J. Minár (2014b), Late Cretaceous–Cenozoic thermal evolution of the northern part of the Central Western Carpathians (Slovakia): Revealed by zircon and apatite fission track thermochronology, *Tectonophysics*, *615*, 142–153, doi:10.1016/j.tecto.2014.01.002.

Krzywiec, P., N. Oszczypko, K. Bukowski, M. Oszczypko-Clowes, M. Śmigielski, F. M. Stuart, C. Persano, and H. D. Sinclair (2014), Structure and evolution of the Carpathian thrust front between Tarnów and Pilzno (Pogórska Wola area)—Results of integrated analysis of seismic and borehole data, *Geol. Q.*, *58*(3), 399–416, doi:10.7306/gq.1189.

Lexa, J., et al. (2000), Geological map of Western Carpathians and adjacent areas: Ministry of Enviroment of the Slovak Republic and Geological Survey of Slovak Republic, scale 1:500 000.

Lock, J., and S. Willett (2008), Low-temperature thermochronometric ages in fold-and-thrust belts, *Tectonophysics*, *456*(3), 147–162, doi:10.1016/j.tecto.2008.03.007.

Lonergan, L., and N. White (1997), Origin of the Betic-Rif mountain belt, *Tectonics*, *16*(3), 504–522, doi:10.1029/96TC03937.

Łoziński, M., A. Wysocka, and M. Ludwiniak (2014), Neogene terrestrial sedimentary environments of the Orava-Nowy Targ Basin: Case study of the Oravica River section near Čimhová, Slovakia, *Geol. Q.*, doi:10.7306/gq.1209.

Ludwiniak, M. (2010), Multistage development of joint-network in the flysch rocks of western Podhale (Inner Western Carpathians, Poland), *Acta Geol. Pol.*, *60*, 283–316.

Mastella, L. (1975), Flysch tectonic in the eastern part of the Podhale Basin (Carpathians, Poland) [in Polish with English summary], *Ann. Soc. Geol. Pol.*, *45*, 361–401.

Meesters, A. G. C. A., and T. J. Dunai (2005), A noniterative solution of the (U-Th)/He age equation, *Geochem. Geophys. Geosyst.*, *6*, Q04002, doi:10.1029/2004GC000834.

Narr, W., and J. Suppe (1994), Kinematics of basement-involved compressive structures, *Am. J. Sci.*, *294*(7), 802–860.

Nemčok, J., et al. (1994), Geologická Mapa Tatier (Geological Map of the Tatra Mountains), 1: 50 000, Geologický Ústav Dionýza Štúra, Bratislava.

Nemčok, M., G. Pogácsás, and L. Pospíšil (2006a), Activity timing of the main tectonic systems in the Carpathian–Pannonian region in relation to the rollback destruction of the lithosphere, in *The Carpathians and Their Foreland: Geology and Hydrocarbon Resources: AAPG Memoir*, vol. 84, edited by J. Golonka and F. J. Picha, pp. 743–766, doi:10.1306/985627M843083.

Nemčok, M., L. Pospíšil, I. Hrušecký, T. Zsíros (2006b), Subduction in the remnant Carpathian Flysch Basin, in *The Carpathians and Their Foreland: Geology and Hydrocarbon Resources, AAPG Memoir*, vol. 84, edited by J. Golonka and F. J. Picha, pp. 767–785, doi:10.1306/985627M843083.

Oglesby, D. D. (2005), The dynamics of strike-slip step-overs with linking dip-slip faults, *Bull. Seismol. Soc. Am.*, *95*(5), 1604–1622, doi:10.1785/0120050058.

Oszczypko, N. (2006), Late Jurassic-Miocene evolution of the Outer Carpathian fold-and-thrust belt and its foredeep basin (Western Carpathians, Poland), *Geol. Q.*, *50*(1), 169–194.

Oszczypko N., P. Krzywiec, I. Popadyuk and T. Peryt (2006), Carpathian Foredeep Basin (Poland and Ukraine): Its sedimentary, structural and geodynamic evolution, in *The Carpathians and Their Foreland: Geology and Hydrocarbon Resources, AAPG Memoir*, vol. 84, edited by J. Golonka and F. J. Picha, pp. 293–350, doi:10.1306/985612M843072.

Oszczypko, N., E. Jurewicz, and D. Plašienka (2010), Tectonics of the Klippen Belt and Magura nappe in the Eastern part of the Pieniny Mts (Western Carpathians, Poland and Slovakia): New approaches and results, Scientific Annals, School of Geology, Aristotle University of Thessaloniki, Proceedings of the XIX CBGA Congress, Thessaloniki, Greece, 100, 221–229.

Petrík, I., P. Nabelek, M. Janák, and D. Plašienka (2003), Condition of formation and crystallization kinetics of highly oxidized pseudotachylytes from the High Tatras (Slovakia), *J. Petrol.*, *44*(5), 901–927, doi:10.1093/petrology/44.5.901.

Plašienka, D., P. Grecula, M. Putiš, M. Kováč, and D. Hovorka (1997), Evolution and structure of the Western Carpathians: An overview, in *Geological Evolution of the Western Carpathians*, *Mineralia Slovaca*, edited by P. Grecula et al., pp. 1–24.

Plašienka, D., M. Janák, and I. Petrík (2001), Excursion to the Tatra Mountains, Central Western Carpathians: Tectonometamorphic Records of Variscan and Alpine Orogeny, *Geolines*, *13*, 141–148.

Plašienka, D., I. Broska, D. Kissová, and I. Dunkl (2007), Zircon fission-track dating of granites from the Vepor–Gemer Belt (Western Carpathians): Constraints for the Early Alpine exhumation history, *J. Geosci.*, *52*, 113–123, doi:10.3190/jgeosci.009.

Platt, J. P., and P. C. England (1994), Convective removal of lithosphere beneath mountain belts; thermal and mechanical consequences, *Am. J. Sci.*, *294*(3), 307–336.

Ratschbacher, L., W. Frisch, H. G. Lintzer, and O. Merle (1991), Lateral extrusion in the Eastern Alps. Part 2. Structural analysis, *Tectonics*, *10*, 257–271, doi:10.1029/90TC02623.

Reiners, P. W., and M. T. Brandon (2006), Using thermochronology to understand orogenic erosion, *Annu. Rev. Earth Planet. Sci.*, *34*, 419–466, doi:10.1146/annurev.earth.34.031405.125202.

Roniewicz, P. (1969), Sedymentacja eocenu numulitowego Tatr, *Acta Geol. Pol.*, *19*(3), 503–608.

Royden, L., F. Horváth, A. Nagymarosy, and L. Stegena (1983), Evolution of the Pannonian basin system: 2. Subsidence and thermal history, *Tectonics*, *2*, 91–137, doi:10.1029/TC002i001p00091.

Rubinkiewicz, J., and M. Ludwiniak (2005), Fracture and fault development in Werfenian quartzitic sandstones—A case study from the autochthonous cover of the Tatra Mts. (Poland), *Ann. Soc. Geol. Pol.*, *75*, 171–187.

Schmid, S. M., D. Bernoulli, B. Fügenschuh, L. Matenco, S. Schaefer, R. Schuster, M. Tischler, and K. Ustaszewski (2008), The Alpine-Carpathian-Dinaridic orogenic system: Correlation and evolution of tectonic units, *Swiss J. Geosci.*, *101*, 139–183, doi:10.1007/s00015-008-1247-3.

Seghedi, I., H. Downes, S. Harangi, P. R. D. Mason, and Z. Pécskay (2005), Geochemical response of magmas to Neogene–Quaternary continental collision in the Carpathian–Pannonian region: A review, *Tectonophysics*, *410*, 485–499, doi:10.1016/j.tecto.2004.09.015.

Ślączka, A., S. Krugłov, J. Golonka, N. Oszczypko, and I. Popadyuk (2005), Geology and hydrocarbon resources of the Outer Carpathians, Poland, Slovakia, and Ukraine: General Geology, in *The Carpathians and Their Foreland: Geology and Hydrocarbon Resources: AAPG Memoir*, vol. 84, edited by J. Golonka and F. J. Picha, pp. 221–258, doi:10.1306/985610M843070.

Soták, J. (2010), Paleoenvironmental changes across the Eocene-Oligocene boundary: Insights from the Central-Carpathian Paleogene Basin, *Geol. Carpath.*, *61*(5), 393–418, doi:10.2478/v10096-010-0024-1.

Soták, J., M. Pereszlenyi, R. Marschalko, J. Milicka, and D. Starek (2001), Sedimentology and hydrocarbon habitat of the submarine-fan deposits of the Central Carpathian Paleogene Basin (NE Slovakia), *Mar. Pet. Geol.*, *18*, 87–114, doi:10.1016/S0264-8172(00)00047-7.

Sperner, B. (1996), Computer programs for the kinematic analysis of brittle deformation structures and the Tertiary evolution of the Western Carpathians (Slovakia), Tübingen Geowissenschaftliche Arbeiten, Reihe A., 27, 1–81.

Sperner, B., L. Ratsbacher, and M. Nemčok (2002), Interplay between subduction retreat and lateral extrusion: Tectonics of the Western Carpathians, *Tectonics*, *21*, 1051–1075, doi:10.1029/2001TC901028.

Środoń, J., M. Kotarba, A. Biroň, P. Such, N. Clauer, and A. Wójtowicz (2006), Diagenetic history of the Podhale-Orava Basin and the underlying Tatra sedimentary structural units (Western Carpathians): Evidence from XRD and K-Ar of illite-smectite, *Clay Miner.*, *41*, 751–774, doi:10.1180/0009855064130217.

Starek, D., L. Sliva, and R. Vojtko (2012), Eustatic and tectonic control on late Eocene fan delta development (Orava Basin, Central Western Carpathians), *Geol. Q.*, *56*(1), 67–84.

Stockli, D. F. (2005), Application of low-temperature thermochronometry to extensional tectonic settings, *Rev. Mineral. Geochem.*, *58*(1), 411–448, doi:10.2138/rmg.2005.58.16.

Szaniawski, R., M. Ludwiniak, and J. Rubinkiewicz (2012), Minor counterclockwise rotation of the Tatra Mountains (Central Western Carpathians) as derived from paleomagnetic results achieved in hematite-bearing Lower Triassic sandstones, *Tectonophysics*, *560–561*, 51–61, doi:10.1016/j.tecto.2012.06.027.

Tari, G. C., and F. Horváth (2005), Alpine evolution and hydrocarbon geology of the Pannonian Basin: An overview, in *The Carpathians and Their Foreland: Geology and Hydrocarbon Resources: AAPG Memoir*, vol. 84, edited by J. Golonka and F. J. Picha, pp. 605–618, doi:10.1306/985733M843141.

Tokarski, A. K., A. Świerczewska, W. Zuchiewicz, D. Starek, and L. Fodor (2012), Quaternary exhumation of the Carpathians: A record from the Orava-Nowy Targ Intramontane Basin, Western Carpathians (Poland and Slovakia), *Geol. Carpath.*, *63*(4), 257–266, doi:10.2478/v10096-012-0021-7.

Tomaszczyk, M., J. Rubinkiewicz, and A. Borecka (2009), Geological 3D spatial model of the nummulitic Eocene between Mała Łąka and Lejowa valleys in Tatra Mts. [in Polish with English summary], *Przegl. Geol.*, *57*, 69–71.

Vermeesch, P. (2010), HelioPlot, and the treatment of overdispersed (U–Th–Sm)/He data, *Chem. Geol.*, *271*, 108–111, doi:10.1016/j.chemgeo.2010.01.002.